

TOOLS

Dissecting protein tyrosine phosphatase signaling by engineered chemogenetic control of its activity

Jordan Fauser¹, Vincent Huyot¹, Jacob Matsche¹, Barbara N. Szyнал¹, Yuri Alexeev², Pradeep Kota³, and Andrei V. Karginov¹

Protein tyrosine phosphatases (PTPases) are critical mediators of dynamic cell signaling. A tool capable of identifying transient signaling events downstream of PTPases is essential to understand phosphatase function on a physiological time scale. We report a broadly applicable protein engineering method for allosteric regulation of PTPases. This method enables dissection of transient events and reconstruction of individual signaling pathways. Implementation of this approach for Shp2 phosphatase revealed parallel MAPK and ROCK II dependent pathways downstream of Shp2, mediating transient cell spreading and migration. Furthermore, we show that the N-SH2 domain of Shp2 regulates MAPK-independent, ROCK II-dependent cell migration. Engineered targeting of Shp2 activity to different protein complexes revealed that Shp2-FAK signaling induces cell spreading whereas Shp2-Gab1 or Shp2-Gab2 mediates cell migration. We identified specific transient morphodynamic processes induced by Shp2 and determined the role of individual signaling pathways downstream of Shp2 in regulating these events. Broad application of this approach is demonstrated by regulating PTP1B and PTP-PEST phosphatases.

Introduction

Protein tyrosine phosphorylation mediates a variety of cellular processes by affecting enzyme activity, protein localization, and the formation of specific signaling complexes. Protein tyrosine kinases have been studied in depth for their roles in physiological and pathological conditions. However, protein tyrosine phosphatases (PTPs) have proven more enigmatic while remaining highly important for regulation of critical tyrosine phosphorylation (Tiganis and Bennett, 2007; Tonks, 2013; Tonks and Neel, 2001). Particularly challenging is identification of dynamic events triggered by a phosphatase immediately after its activation. Conventional approaches, such as expression of a constitutively active or catalytically dead phosphatase, lack temporal control and can only provide information on the long-term effects of these phosphatases. While specific and bioavailable phosphatase inhibitors have been developed (Liu et al., 2020; Liu et al., 2019; Ran et al., 2016; Vazhappilly et al., 2019), these too have limitations. Specific inhibitors provide temporal control over activity but reveal only how the cell responds to a loss of phosphatase activity. Thus, the current toolset for protein phosphatases remains limited and dissecting the dynamic effects of phosphatase signaling still presents a challenge.

Src homology-2 (SH2) domain-containing protein tyrosine phosphatase 2, Shp2, is a ubiquitously expressed phosphatase containing two tandem SH2 domains, a phosphatase domain,

and a flexible C-terminal tail (Sun et al., 2013; Guo and Xu, 2020). Regulation of Shp2 within cells is dictated by the autoinhibitory interaction between the N-SH2 domain and the phosphatase domain. This autoinhibition is disrupted through N-SH2 binding of phosphorylated tyrosine on Shp2-interacting partners (Anselmi and Hub, 2020; Benjamin et al., 2003). The canonical function of Shp2 is activation of the mitogen-activated protein kinase (MAPK) signaling cascade, Ras-Raf-MEK-ERK. This pathway is dysregulated in many RASopathies such as Noonan syndrome, Noonan syndrome with multiple lentigines, and juvenile myelomonocytic leukemia (Matozaki et al., 2009; Schaeper et al., 2000; Serra-Nedelec et al., 2012; Tajan et al., 2015; Yu et al., 2013). Shp2 also contributes to the regulation of cell migration and cell adhesion to extracellular matrix (Cao et al., 2019; Grosskopf et al., 2015; Hartman et al., 2013; Huang et al., 2012; Lee et al., 2013; Mañes et al., 1999; Sausgruber et al., 2015). However, these processes are dynamic and often transient in nature. Thus, dissection of Shp2-mediated cell migration, adhesions, and protrusions requires tools that enable tight temporal control of its activity. Such tools will uncover short-term and long-term effects of Shp2 activation in regulation of physiological and pathological processes. In addition to the critical role of timing, functions of Shp2 are also dictated by the plethora of signaling complexes it forms. Defining the role of

¹Department of Pharmacology and Regenerative Medicine, University of Illinois at Chicago, Chicago, IL; ²Argonne National Laboratory, Lemont, IL; ³Marsico Lung Institute, University of North Carolina at Chapel Hill, Chapel Hill, NC.

Correspondence to Andrei V. Karginov: karginov@uic.edu.

© 2022 Fauser et al. This article is distributed under the terms of an Attribution–Noncommercial–Share Alike–No Mirror Sites license for the first six months after the publication date (see <http://www.rupress.org/terms/>). After six months it is available under a Creative Commons License (Attribution–Noncommercial–Share Alike 4.0 International license, as described at <https://creativecommons.org/licenses/by-nc-sa/4.0/>).

specific Shp2-mediated signaling complexes is needed to understand how Shp2 regulates different cellular processes. However, these studies are challenging due to paucity of tools for manipulation of Shp2 signaling.

Engineered allosteric regulation offers unique advantages in studying cell signaling due to its temporal and specific control of a protein of interest (Hongdusit et al., 2020; Karginov et al., 2010; Karginov et al., 2014). A chemogenetic approach, the Rapamycin Regulated (RapR) system, has been successfully applied to regulate specific kinase activity to investigate dynamic signaling events (Chu et al., 2014; Karginov et al., 2010; Karginov et al., 2014; Klomp et al., 2019). The RapR system utilizes rapamycin-mediated dimerization of FRB and an insertable FKBP12 (iFKBP) to modulate the activity of a protein of interest. Inserting a highly dynamic iFKBP switch into the catalytic domain of a protein of interest results in allosteric disruption of critical catalytic residues (Karginov et al., 2010). Stabilization of iFKBP upon rapamycin and FRB binding recovers catalytic function and acutely activates the protein of interest. Precise temporal control of activation enables investigation of dynamic signaling events downstream of a specific protein.

We sought to overcome the limitations of current tools for studying phosphatases by developing a method for manipulation of phosphatase activity with tight temporal control and ability to control phosphatases within specific signaling complexes. Utilizing the RapR system, we engineered and optimized allosterically regulated Shp2, PTP1B, and PTP-PEST tyrosine phosphatases. We then implemented RapR-Shp2 to investigate dynamic Shp2 signaling and the specific role of Shp2 in cell migration and spreading. Using this system, we revealed transient morphological changes following the activation of RapR-Shp2 that could not be recapitulated with constitutively active (CA) Shp2. This tool also enabled interrogation of possible parallel Shp2-dependent signaling pathways mediating these dynamic morphological changes.

Results

Design of rapamycin-regulated Shp2 (RapR-Shp2)

We aimed to develop an allosterically regulated Shp2 using rapamycin-induced dimerization of iFKBP and FRB (Fig. 1 A; Karginov et al., 2010). Insertion of the highly dynamic iFKBP switch within the catalytic domain disrupts the catalytic function in the absence of rapamycin. Activity is recovered following the addition of rapamycin and stabilization of iFKBP by FRB/rapamycin binding (Fig. 1 A). To eliminate autoinhibitory regulation and dependence on upstream endogenous pathways of Shp2, we employed a previously described activating mutation (D61A), this ensured activation solely by rapamycin (Chichger et al., 2015; Qiu et al., 2014). Three potential insertion sites were identified in flexible loops within the Shp2 catalytic domain: Val⁴⁰⁶, Thr²⁸⁸, and Lys³¹⁷ (Fig. 1 B). The insertion sites were selected for their structural coupling to catalytically relevant regions (WPD for Val⁴⁰⁶, substrate-binding loop for Thr²⁸⁸ and Lys³¹⁷), while also avoiding potential steric disruption of SH2 domain-mediated protein-protein interactions. The difference in length of the unstructured insertion loops allowed us to test how varying degrees of flexibility affect allosteric control by iFKBP. Both Thr²⁸⁸ and Val⁴⁰⁶ are in shorter

unstructured loops while Lys³¹⁷ is in a long unstructured loop. In the shorter Val⁴⁰⁶ and Thr²⁸⁸ insertion loops, an additional secondary structure disruptor, Gly residue, was added at the junction of Shp2 and iFKBP. Previous studies indicated that insertion of short linkers such as Gly or G-S/P-G can improve the regulation of catalytic function through decreased disruption of protein structure by iFKBP insertion (Karginov et al., 2010). Using a cell-free in vitro assay with immunoprecipitated Shp2 and purified phosphorylated N-terminal fragment of paxillin, we identified Val⁴⁰⁶ insertion site as the best candidate for allosteric regulation of Shp2 phosphatase activity (Fig. 1, C and D). Insertion of iFKBP at the Thr²⁸⁸ site failed to fully activate the phosphatase with rapamycin treatment (Fig. 1, C and D). The Lys³¹⁷ site retained phosphatase activity in the absence of rapamycin (Fig. 1, C and D). Thus, the length of the insertion loop and proximity to catalytic residues are correlated with the dynamic range of regulation, where shorter loops enabled tighter regulation of catalytic activity.

Engineered Shp2 with iFKBP insertion at Val⁴⁰⁶ retained low residual activity in the absence of rapamycin as compared to dominant negative (DN) Shp2 (Fig. 1, C and D). Thus, to optimize the regulation of this construct, we further modified the linkers connecting iFKBP to Shp2 at Val⁴⁰⁶. Previous work using the RapR system in kinases demonstrated the importance of these linkers in optimized control of catalytic function (Karginov et al., 2010). The flexibility of the linkers was modified by insertion of an additional Gly-Ser-Gly fragment and truncation of Shp2 amino acids 405 and 407 on each side of iFKBP insert (Fig. 2 A). Coupling a longer GSG linker with deletion of amino acids 405–407 resulted in the best disruption of phosphatase activity in the absence of rapamycin and best recovery of activity in the presence of rapamycin (Fig. 2, B and C). For simplicity, this optimized version, with the replacement of residues 405–407 by iFKBP with GSG linkers, will be referred to as RapR-Shp2. Evaluation of substrate dephosphorylation over time revealed that RapR-Shp2 exhibits kinetics comparable to CA-Shp2 (Fig. 2, D and E). Our analysis estimated 1.2-fold increase in K_m and 2.2-fold increase in V_{max} suggesting only a small reduction in substrate binding affinity while catalytic efficiency was retained.

In silico prediction of allosteric regulation by iFKBP insertion

To interrogate the potential mechanistic effect of iFKBP on the catalytic domain of Shp2, we performed molecular dynamics simulations of RapR-Shp2 with and without FRB and rapamycin, and the wild-type Shp2 catalytic domain. These simulations facilitated the analysis of the potential effect of the iFKBP insertion on substrate recognition or substrate coordinating loops within Shp2. In the absence of rapamycin, the highly dynamic iFKBP insertion increases the root-mean-square fluctuation (RMSF) throughout the catalytic domain, suggesting increased structural plasticity that could disrupt activity (Fig. 3, A and B). Simulations of the RapR-Shp2-rapamycin-FRB complex reveal an overall decrease in RMSF, suggesting stabilization of this domain and potential recovery of catalytic function (Fig. 3, A and C). The substrate binding loop containing the KNRY sequence shows the greatest difference between wild-type Shp2 and unbound RapR-Shp2, while the WPD loop and catalytic residues do not appear to be affected by the insertion (Fig. 3, A–D). The RMSF of the

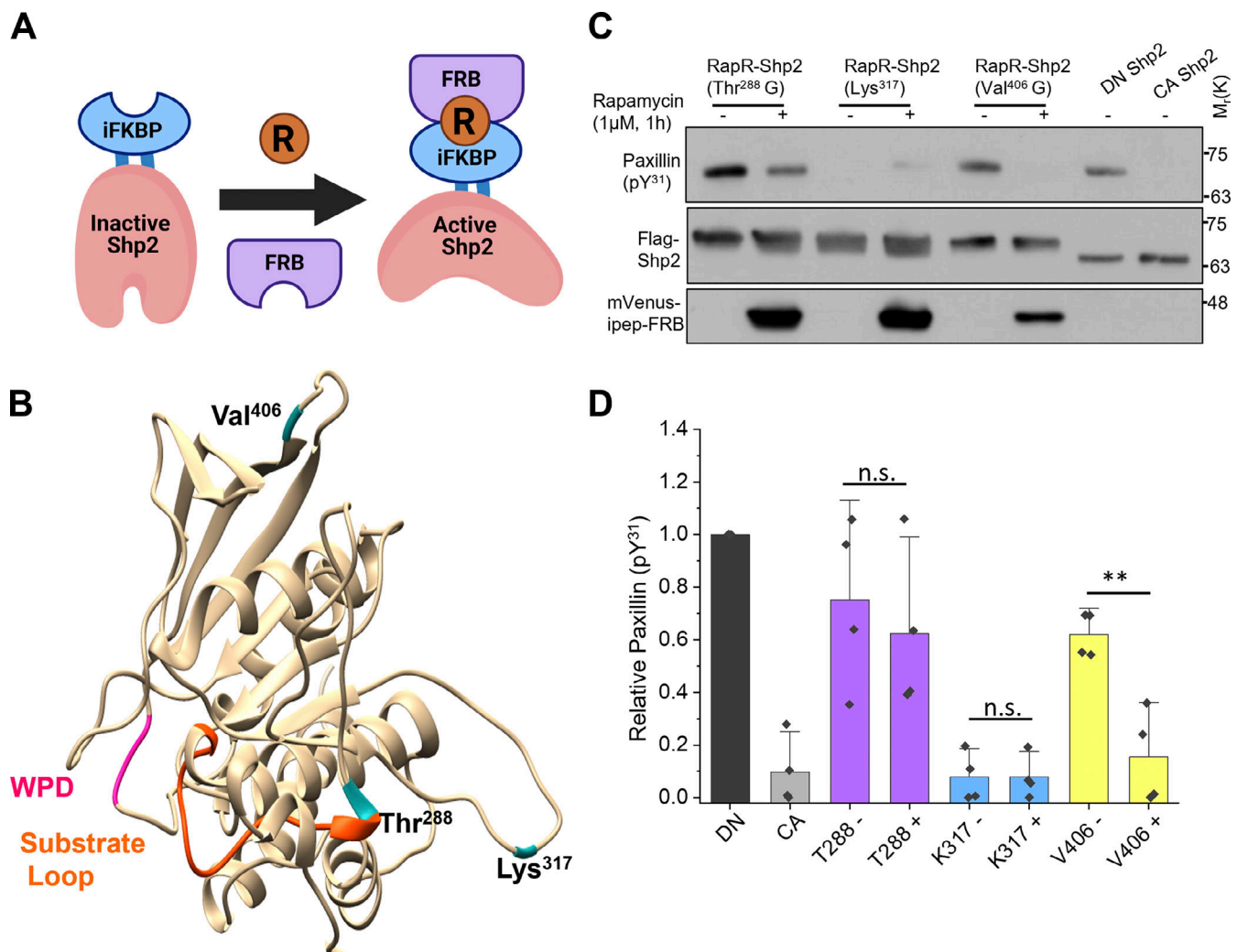


Figure 1. Design of RapR-Shp2 and in vitro analysis of phosphatase activity. (A) Representation of RapR-Shp2. Insertion of iFKBP (blue) allosterically disrupts the phosphatase domain (peach). Activity is restored following rapamycin (orange) and FRB (purple) binding. Created using biorender.com. (B) Phosphatase domain of Shp2 (PDB accession no. 4DGP, beige) with indicated potential insertion sites (blue), WPD loop (magenta), and substrate binding loop containing KRNY sequence (orange). (C and D) Cell-free in vitro assay evaluating phosphatase activity through dephosphorylation of phospho-paxillin substrate. Activity analysis of immunoprecipitated constitutively active Shp2 (CA-Shp2), dominant negative Shp2 (DN-Shp2), and RapR-Shp2 constructs (iFKBP insertion sites Thr²⁸⁸, Lys³¹⁷, Val⁴⁰⁶) with and without rapamycin. Representative blots of N = 4 independent experiments shown with quantification of Paxillin (pY³¹) blot intensity (D). Error bars represent 90% confidence interval (CI). Analysis of statistical significance at the 0.05 level was determined by two-tailed Student's *t* test for independent pairwise comparisons of each insertion site with and without rapamycin. *P < 0.05, **P < 0.01.

catalytic domain of RapR-Shp2-rapamycin-FRB complex, including the substrate binding loop, closely resembles that of the wild-type catalytic domain of Shp2 (Fig. 3, C and D). We observed the loop immediately adjacent to the substrate binding loop exhibited elevated RMSF even after complexation with FRB and rapamycin. This may contribute to reduced substrate binding in the RapR-Shp2 as was observed in our kinetics analysis. These results reveal a potential mechanism of allosteric regulation of Shp2 through dynamic disruption of the substrate binding regions of the catalytic domain as well as provide information on the effect of the RapR insertion on catalytic efficiency.

Validation of RapR-Shp2 phosphatase activity and signaling
Shp2 is well established to activate the Ras-Raf-MEK-ERK pathway downstream of growth factor signaling (Benjamin

et al., 2010; Benjamin et al., 2003; Meng et al., 2005; Vazhappilly et al., 2019). Overexpression of CA-Shp2 (D61A) increases levels of active ERK1/2 (Yang et al., 2019). To validate that RapR-Shp2 can emulate Shp2 signaling, we activated overexpressed RapR-Shp2 in HEK293T cells (Fig. S1, D and E). Following activation for an hour, RapR-Shp2 induced ERK phosphorylation comparable to the effect of CA-Shp2 (Fig. 4 A and Fig. S1 A). In the absence of rapamycin, RapR-Shp2 expressing cells showed basal levels of ERK phosphorylation (Fig. 4 A and Fig. S1 A). Thus, our engineered RapR-Shp2 tool can induce canonical Shp2 signaling in live cells.

Activation of ERK 1/2 indicates that RapR-Shp2 likely recognizes endogenous substrates and forms canonical protein-protein interactions. To further validate these functions, we assessed whether RapR-Shp2 mediates dephosphorylation of

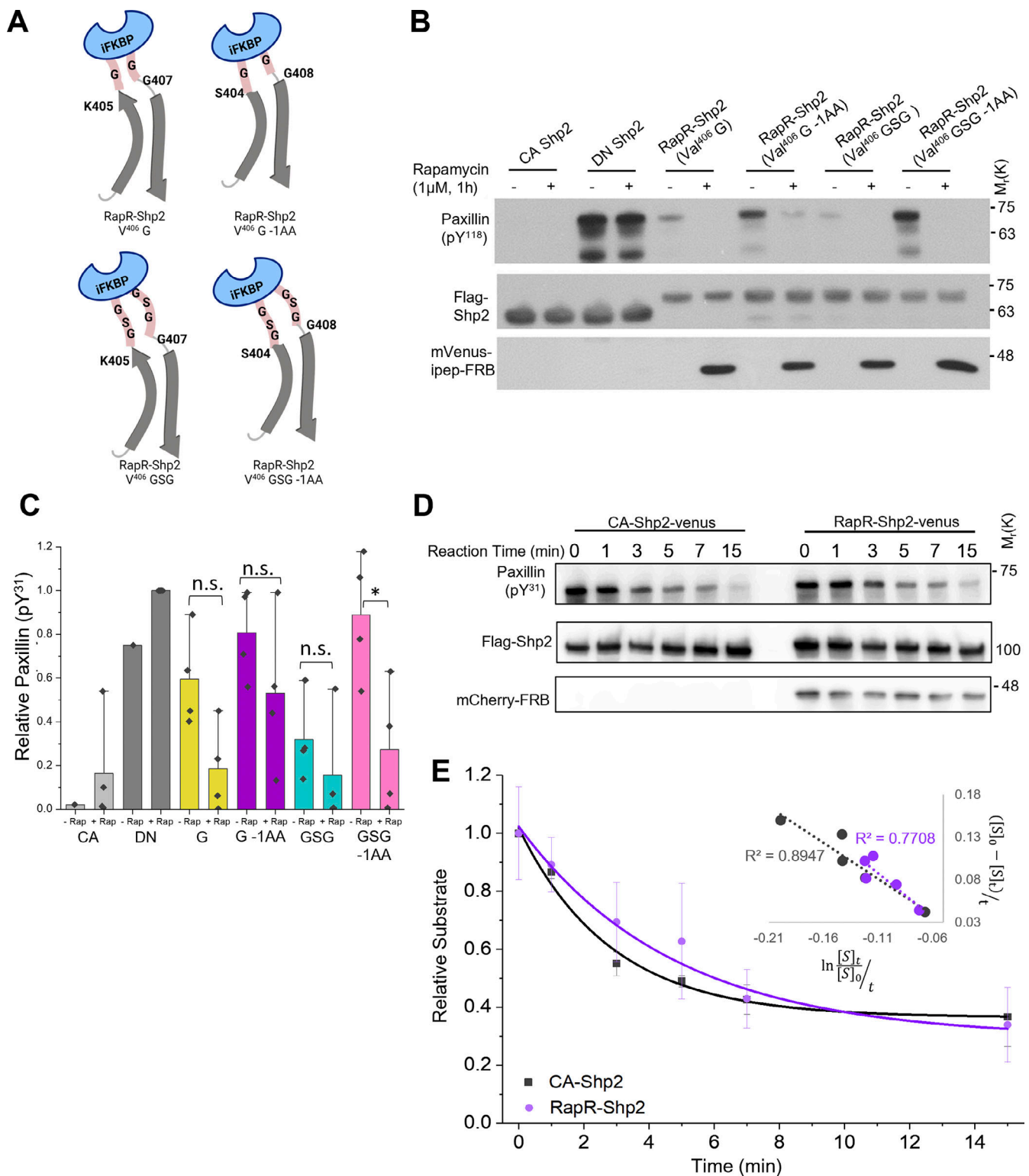


Figure 2. **Optimization of RapR-Shp2 through flexible linker modifications.** (A) Representation of the linker modifications for RapR-Shp2 showing Shp2 β -strands (gray, insertion site residues are indicated), flexible linkers (pink) and iFKBP (blue). Created using biorender.com. (B and C) Cell-free in vitro assay evaluating phosphatase activity of RapR-Shp2 Val⁴⁰⁶ insertion site with varied flexible linkers between iFKBP and the catalytic domain. Four variants depicted in Fig. 2 A were tested. Indicated constructs were immunoprecipitated and their ability to dephosphorylate purified phosphorylated paxillin was assessed in vitro. Representative blots of $N = 4$ independent experiments shown with quantification of Paxillin (pY¹¹⁸) blot intensity (C). Analysis of statistical significance at the 0.05 level was determined by two-tailed Student's t test for independent pairwise comparisons of each linker with and without rapamycin. * $P < 0.05$. (D and E) Comparison of RapR-Shp2 and CA-Shp2 phosphatase activity. Activated RapR-Shp2 and CA-Shp2 were immunoprecipitated and incubated with purified phospho-paxillin for the indicated time. Activity assessed via immunoblot of phospho-Paxillin (pY³¹). Representative blot of $N = 3$ independent experiments. (E) Phosphatase activity plot showing relative change in substrate over time and exponential decay fit curve. Insert shows plot of the integrated

rate equation derived to obtain relative K_m and V_{max} values (the slope and the intercept of the linear plot) using approach described in Orsi and Tipton (1979). RapR-Shp2 shows 1.2 increase in K_m and 2.2 increase in V_{max} when compared to CA-Shp2. All error bars show 90% CI.

known Shp2 substrates in live cells. Here, we used A431 cells because of their enhanced EGFR activity. Activation of RapR-Shp2 in these cells resulted in dephosphorylation of several established Shp2 substrates: EGFR (Y^{992}), FAK (Y^{576}/Y^{577}), PLC γ (Y^{783}), ROCK II (Y^{722}), and Gab1 (Y^{627} and Y^{659} ; Fig. 4 B and Fig. S1 B, D, and E; Agazie and Hayman, 2003; Cunnick et al., 2001; Lee and Chang, 2008; Ren et al., 2011; Tsutsumi et al., 2006; Vidyasiri Vemulapalli et al., 2019 Preprint; Witsenburg et al., 2013). In addition, we ensured that insertion of iFKBP into the catalytic domain did not disrupt the function of SH2 domains of Shp2. This was established by evaluating protein-protein interactions of RapR-Shp2 with Gab1, a known binding partner for both Shp2 SH2 domains, as well as a known substrate and binding partner EGFR (Fig. 4 C and Fig. S1 C; Agazie and Hayman, 2003; Cunnick et al., 2001; Hartman et al., 2020). These data validated the ability of RapR-Shp2 to emulate wild-type Shp2 phosphatase activity and protein-protein interactions in living cells.

Induction of transient morphological changes in HeLa cells by acute Shp2 activation

Shp2 is implicated in cell migration and spreading both through upstream signaling and direct regulation of focal adhesions and cytoskeletal rearrangements (Cao et al., 2019; Grosskopf et al., 2015; Hartman et al., 2013; Huang et al., 2012; Lee et al., 2013; Mañes et al., 1999; Mizutani et al., 2007; Ren et al., 2004; Sausgruber et al., 2015; Tan et al., 2019; Tsutsumi et al., 2006; Wu et al., 2016; Yu et al., 1998; Zhang et al., 2013). However, due to the approaches employed in these studies, the specific transient effects of Shp2 activation on cell morphology were not established. Application of RapR-Shp2 allowed us to overcome these limitations. We evaluated the effects of Shp2 activation on several morphological processes defining cell morphodynamics: formation and retraction of broad lamellipodia-like protrusions, cell spreading, and cell migration. Activation of RapR-Shp2 in HeLa cells led to immediate stimulation of cell spreading and protrusive activity (Fig. 5, A and B; Fig. S1, D and E; and Fig. S2 A). Cell spreading stops 30 min after activation (Fig. 5, A and C) coinciding with an increase in cell retraction (Fig. 5 D and Fig. S2 B). These events were accompanied by a transient increase in cell migration which returned to basal levels after 3 h of RapR-Shp2 activity in HeLa cells (Fig. 5 E and Video 1). HeLa cells expressing only FRB did not exhibit these morphological changes in response to rapamycin (Fig. 5, A–E; and Fig. S2, A and B). Furthermore, cells expressing CA-Shp2 (D61A; Fig. S2 E) did not exhibit increased basal migration or significant changes in spreading or migration after rapamycin treatment (Fig. S2, C and D). RapR-Shp2 was showing same diffused localization pattern as CA-Shp2 (Fig. S2 E). Thus, RapR-Shp2 revealed a series of transient morphological changes which can be observed only through acute Shp2 activation.

MEK/ERK dependence in RapR-Shp2-induced spreading and RapR-Shp2-mediated ERK-independent migration

Activation of ERK has previously been established to contribute to cell spreading and migration (Tanimura and Takeda, 2017). As

Shp2 canonically activates ERK, we reasoned that Shp2-induced spreading and migratory phenotypes may be mediated through activation of ERK. Inhibition of MAPK signaling through the use of a MEK or ERK1/2 inhibitors, trametinib (Rutkowski et al., 2015), and FR180204, respectively (Ohori et al., 2005), resulted in ablation of RapR-Shp2-induced cell spreading (Fig. 6, A and B). However, some cell migration persisted in the absence of ERK activity (Fig. 6 C). In addition, increased protrusion and retraction activity are observed despite ERK inhibition, though trametinib-treated cells exhibit a 10-min delay in induction of protrusive activity (Fig. 6, D–F). These results suggest a parallel ERK-independent pathway for Shp2-mediated protrusions and cell migration.

N-terminal SH2 domain of Shp2 mediation of ERK-independent migration and protrusive activity through a parallel ROCK II pathway

Shp2 catalytic function is a critical mediator of signaling in cells. However, the specificity of individual pathways downstream of Shp2 is often mediated by its SH2 domains (Anselmi et al., 2020; Barua et al., 2007; Benjamin et al., 2010; Meng et al., 2005; Paardekooper Overman et al., 2014; Sha et al., 2013; Guo and Xu, 2020; Wu et al., 2016; Yu et al., 2013). We interrogated the role of each SH2 domain in Shp2-induced morphodynamic changes by introducing previously described R32L and R138L mutations into the SH2 domains of RapR-Shp2, ablating phospho-tyrosine binding of the N- and C-SH2 domains, respectively. This disruption of protein-protein interactions prevents downstream signaling (Sun et al., 2013). Both RapR-Shp2 mutants failed to activate ERK in HEK293 cells, confirming that both SH2 domains are required for stimulation of MAPK pathway (Fig. 7 A and Fig. S3 A; Sha et al., 2013). Activation of the SH2 domain mutants of RapR-Shp2, however, revealed a specific role for the N-SH2 domain in ERK-independent migration. Loss of phospho-tyrosine binding by the N-SH2 domain (R32L) abolished both the spreading and migratory phenotypes while significantly reducing protrusive and retractive activity (Fig. 7, B–F and Fig. S3, B and C). In contrast, the C-SH2 domain mutant (R138L) still induced cell migration, although to a lesser extent than that of wild-type RapR-Shp2 (Fig. 5 E and Fig. 7 D). Furthermore, R138L RapR-Shp2 was incapable of inducing cell spreading (Fig. 7, B and C). These results suggested that the N-SH2 domain alone was sufficient to mediate ERK-independent cell migration. To further confirm this ERK independence, we activated R138L RapR-Shp2 in the presence of trametinib and again observed induction of cell migration, but not cell area increase, following activation (Fig. S3, E–G).

Shp2 can signal through small GTPase RhoA by directly regulating its downstream effector RhoA-dependent kinase, ROCK II, through dephosphorylation of an inhibitory phospho-tyrosine (Lee and Chang, 2008; Xu et al., 2019). Our analysis shows that RapR-Shp2 mediates dephosphorylation of ROCKII in living cells (Fig. 4 B). Thus, this pathway presents a potential

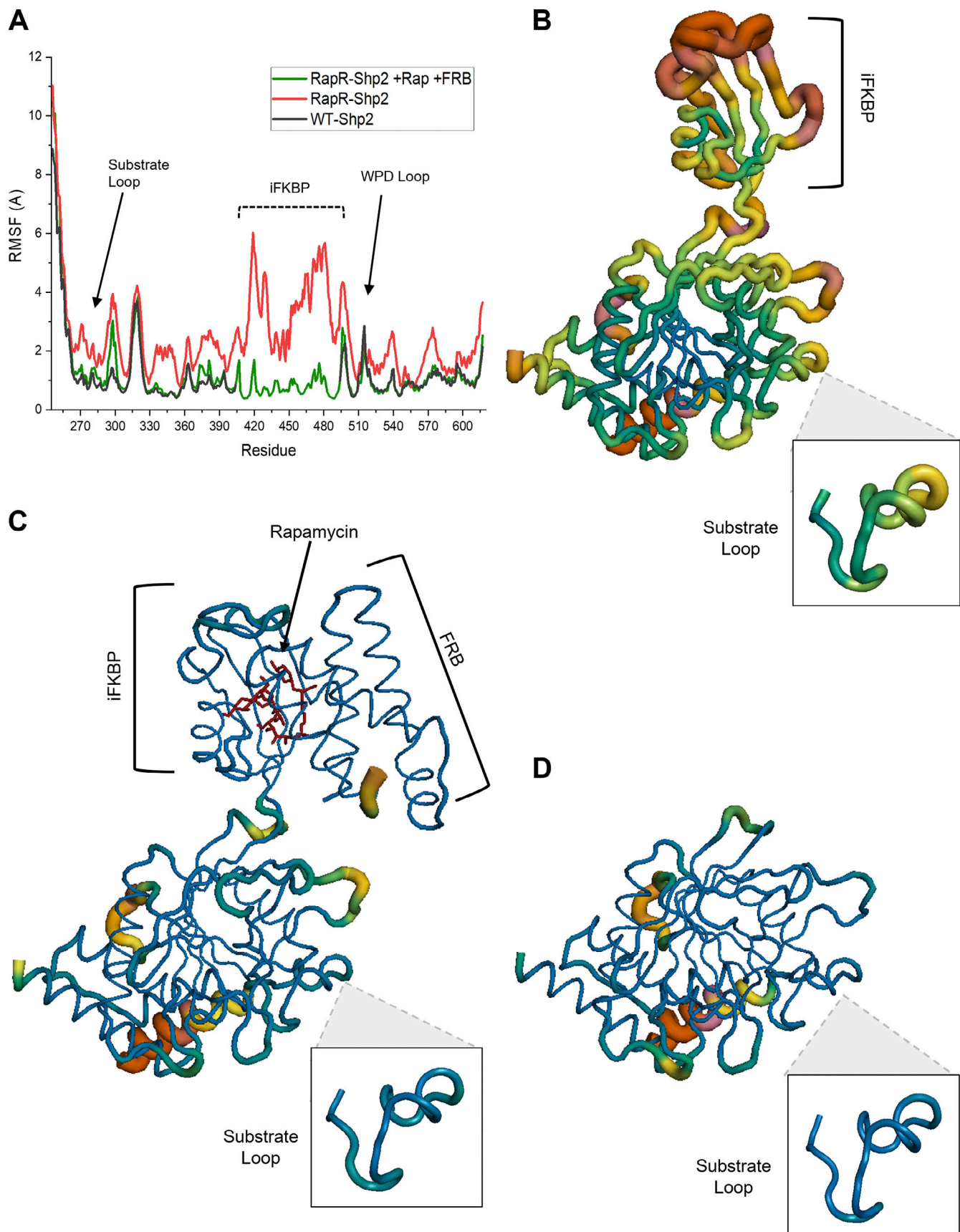


Figure 3. **Molecular dynamics simulations of RapR-Shp2 reveal potential allosteric mechanism of regulation by iFKBP insert.** (A) Root-mean-square fluctuation (RMSF) of individual amino acid residues of RapR-Shp2 in the absence of Rapamycin and FRB (red), RapR-Shp2 bound to Rapamycin and FRB

(green), and wild-type Shp2 (black). Average RMSF values were determined from three 50 ns simulations for each model. **(B–D)** Tube representation of average RMSF (B) RapR-Shp2 without Rapamycin or FRB (PDB accession no. 4GDP for Shp2 and 4FAP for FKBP-Rapamycin-FRB), (C) RapR-Shp2 bound to FRB/Rapamycin, and (D) Wild-type Shp2. Tube thickness and color correspond to increased RMSF. Blue indicates low RMSF, while red colors indicate high RMSF. A zoomed-in representation of the substrate loop is shown in callout.

mechanism for ERK-independent Shp2-mediated regulation of cell migration (Lee and Chang, 2008; Xu et al., 2019). Indeed, inhibition of ROCK II blocked ERK-independent migration induced by the C-SH2 domain mutant of RapR-Shp2 (R138L; Fig. 7 D). R138L RapR-Shp2 still induced protrusive and retractive activity in the presence of ROCK II inhibitor (Fig. 7, E and F; and Fig. S3, D and G). These data suggest that the N-SH2 domain of Shp2 independently mediates the necessary signaling complexes to induce ROCK-dependent migration following activation of Shp2 phosphatase activity.

Dissection of Shp2 signaling using targeted activation of pathways (RapRTAP)

The morphological changes observed with the individual SH2 domain mutants suggest that cell spreading and migration are mediated by Shp2 signaling in different protein complexes. Thus, we investigated Shp2 activation within specific signaling complexes that may contribute to these different morphological changes. One advantage of the RapR system is that the regulated protein of interest can be specifically targeted to a known interacting partner using the RapRTAP method (rapamycin-regulated targeted activation of pathways; Karginov et al., 2014). By fusing FRB to a specific binding partner, the RapR protein can be activated within a designated complex (Fig. 8 A). Thus, we employed the RapRTAP system to dissect the role of Shp2 complex-specific signaling in cell spreading and migration.

Shp2 has been well established to bind GRB2-associated binding (Gab) proteins 1 and 2 leading to Shp2 activation and downstream signaling (Meng et al., 2005; Ren et al., 2004; Schaeper et al., 2000; Zhang et al., 2013). Shp2 is also known to play a role in focal adhesion complexes, with studies identifying Shp2 interactions with a variety of focal adhesion proteins (Hartman et al., 2013; Huang et al., 2012; Lee et al., 2013; Mizutani et al., 2007; Paardekooper Overman et al., 2014; Tan et al., 2019; Tsutsumi et al., 2006; Yu et al., 1998). Furthermore, Shp2 signaling through Gab1, Gab2, and in focal adhesion complexes, has been implicated in regulation of cell spreading and migration (Hartman et al., 2013; Meng et al., 2005; Ren et al., 2004; Zhang et al., 2013). However, the specific contributions of each of these complexes in dynamic morphological changes remain to be dissected. Thus, we interrogated the role of each of these pathways in Shp2-induced morphodynamic changes.

FRB was fused to Gab1 and Gab2 at the N-terminus, enabling rapamycin-mediated recruitment and activation of RapR-Shp2 (Fig. 8 A). We introduced Y628F/Y660F and Y604F/Y634F mutations into Gab1 and Gab2, respectively, to eliminate known Shp2 binding sites and prevent interaction with endogenous protein (Cunnick et al., 2001; Liu et al., 2001). The R32L mutant of RapR-Shp2 was used for targeting since it cannot induce any morphodynamic changes (Fig. 7, B–D). This design ensured that

engineered Shp2-Gab signaling pathway will be regulated only by rapamycin and prevented any influence by endogenous components. Targeting R32L RapR-Shp2 to either mutant Gab1 or Gab2 stimulated an increase in cell area (Fig. 8, B and C; and Fig. S4, G and H). Following the initial increase in protrusions (Fig. 8 D; and Fig. S4, A and C), R32L RapR-Shp2 targeted to Gabs initiated cell migration, showing a significant increase in the path length over the first 2 h after activation (Fig. 8 E; and Videos 2 and 3). This migration occurred concurrently with increases in retractive activity (Fig. S4, B and D). Migration induced by R32L RapR-Shp2 targeted to Gabs was attenuated relative to unmodified RapR-Shp2 activation (Fig. 5 E), suggesting that localization of active Shp2 to Gabs constitutes only a part of Shp2 signaling involved in these morphological changes.

Next, we interrogated the effects of Shp2 signaling in focal adhesions on cell spreading and migration. One of the proposed binding partners and substrates for Shp2 in focal adhesions is FAK, which is phosphorylated at Y³⁹⁷ to facilitate Shp2 association (Chichger et al., 2015; Hartman et al., 2013). Thus, we employed a FAK construct containing FRB inserted at Y³⁹⁷ (FAK(397)-FRB) to recruit RapR-Shp2 to focal adhesions and activate it. Activation of R32L RapR-Shp2 in complex with FAK induced robust cell spreading (Fig. 8, B and C; and Fig. S4 I and Video 4). However, it did not induce cell migration (Fig. 8 E). This signaling pathway stimulated a transient increase in protrusive activity, which occurred concurrently with cell spreading. It failed to induce prolonged protrusive and retractive activity associated with cell migration (Fig. 8 D; and Fig. S4, E and F). These data indicate that Shp2 regulates cell spreading by signaling in focal adhesion complexes.

Our results demonstrate that Shp2-mediated cell spreading depends on ERK activity (Fig. 6, A and B). Activation of R32L RapR-Shp2 in complex with FAK resulted in a transient increase in ERK phosphorylation 10–30 min after the addition of rapamycin (Fig. S5 A), concurrent with the observed cell spreading. This suggests that Shp2 activation in focal adhesions induces cell spreading, at least in part, through activation of ERK. Indeed, inhibition of MEK activity by Trametinib significantly reduced cell spreading triggered by targeting R32L RapR-Shp2 to FAK(397)-FRB (Fig. S5 B). This evidence suggests that Shp2 phosphatase activity within focal adhesions induces cell spreading in a MAPK pathway-dependent manner.

Our data show that targeting the N-SH2 mutant of RapR-Shp2 (R32L) to FAK stimulates ERK activation and cell spreading, but not cell migration (Fig. 8, B, C, and E; and Fig. S5 A). By contrast, the C-SH2 mutant of RapR-Shp2 (R138L) signals through N-SH2 domain to mediate ERK-independent cell migration through ROCK II, but not cell spreading (Fig. 7, B–D). Thus, we hypothesized that the combination of the N-SH2-mediated pathway with Shp2 signaling in focal adhesions should

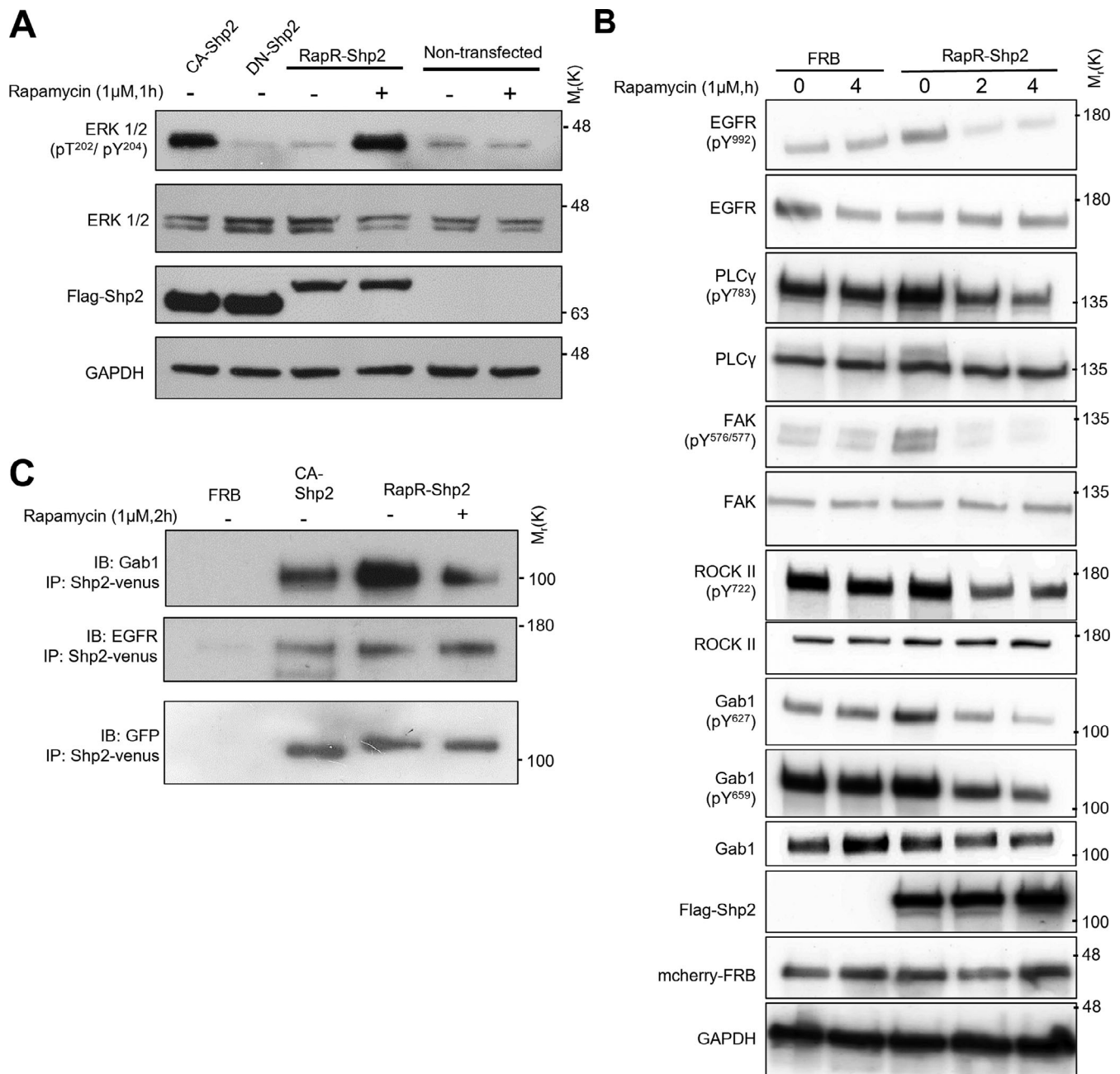


Figure 4. **Validation of optimized RapR-Shp2 phosphatase activity and signaling in living cells.** (A) Immunoblot analysis of ERK activation induced by RapR-Shp2 in HEK293T cells. Cells transiently transfected with CA-Shp2-flag, DN-Shp2-flag, and RapR-Shp2-flag constructs as well as nontransfected cells were treated with rapamycin or ethanol (control) as indicated. Lysates were analyzed by immunoblotting using indicated antibodies. Representative blots of *N* = 3 independent biological replicates. (B) Dephosphorylation of endogenous substrates by RapR-Shp2. A431 cells were transduced with adenoviral RapR-Shp2-mVenus-flag and mCherry-FRB constructs, treated with rapamycin or ethanol (control) for 2 or 4 h, and assessed for phosphorylation of EGFR (pY⁹⁹²), FAK (pY^{576/577}), PLCγ (pY⁷⁸³), ROCK II (pY⁷²²), and Gab1 (pY⁶²⁷ or pY⁶⁵⁹). Representative blots of *N* = 5 independent biological replicates. (C) Validation of RapR-Shp2 protein-protein interactions by coimmunoprecipitation. Lentiviral CA-Shp2-mVenus or adenoviral RapR-Shp2-mVenus were expressed in A431 cells, immunoprecipitated, and the presence of Shp2 interacting proteins, EGFR and Gab1, were assessed by immunoblotting. Representative blots of *N* = 3 (EGFR) and *N* = 6 (Gab1) independent experiments.

induce cell spreading and migration (Fig. 9 A). Indeed, targeting R138L RapR-Shp2 to FAK(397)-FRB stimulated robust and immediate spreading and protrusions (Fig. 9, B and D) as well as induced cell migration (Fig. 9 C and Video 5). Unlike R32L RapR-Shp2 targeted to FAK, elevated protrusive activity was sustained after the initial spike in protrusions (Fig. 9 D). Retraction

activity is also briefly stimulated above basal levels, contrasting the phenotypes observed with R32L RapR-Shp2 (Fig. 9 E). These data indicate that combined N-SH2-mediated protein-protein interactions and phosphatase activity in focal adhesion protein complexes drives both cell spreading and cell migration.

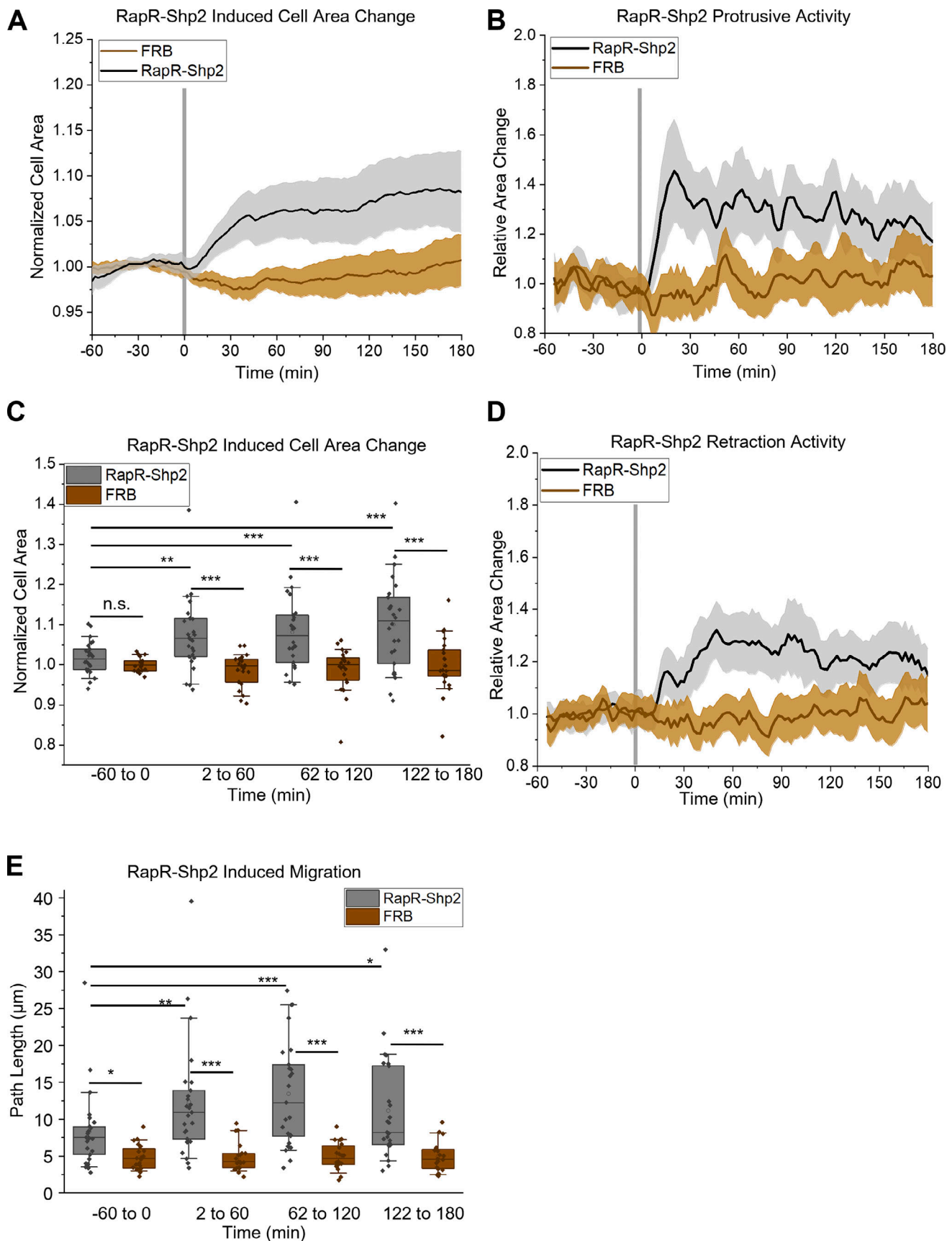


Figure 5. **Transient cell spreading and migration of HeLa cells induced by RapR-Shp2 activation.** HeLa cells transiently expressing mCherry-ipep-FRB alone (control, $N = 22$ cells, two separate biological replicates) or coexpressed with RapR-Shp2-mVenus-flag ($N = 26$ cells, six separate biological replicates)

were stained with CellMask Deep Red membrane marker and imaged live. Images of CellMask were used to assess morphological changes. Rapamycin was added at 0 min (gray line in A, B, and D). **(A and B)** Analysis of changes in cell area (A) and Protrusive Activity (B) for cells expressing RapR-Shp2 and FRB (black line) or FRB alone (brown line). Shaded area represents 90% CI. **(C)** Change in cell area induced by activation of Shp2 (gray) compared to FRB control (brown) binned over 1 h intervals. RapR-Shp2 caused significant change in spreading ($F[3,1] = 12.69$, $P < 0.001$) and significant induction over FRB control ($F = 8.80$, $P < 0.001$). FRB control cells exhibited no significant change in cell area over time ($F[3,1] = 1.19$, $P = 0.32$). **(D)** Analysis of retraction activity for cells expressing RapR-Shp2 and FRB (black line) or FRB alone (brown line). Shaded area represents 90% CI. **(E)** Change in cell migration induced by activation of RapR-Shp2 (gray) compared to FRB alone control (brown) (shown as path length over 1 h intervals). RapR-Shp2 caused significant change in migration relative to basal at all time points ($F[3,1] = 7.50$, $P < 0.001$) and significant induction over FRB control ($F = 28.03$, $P < 0.001$). FRB control cells exhibited no significant change in cell migration over time ($F[3,1] = 0.08$, $P = 0.97$). (C and E) Box and whisker plots: Box indicates first through third quartile with median line, whiskers are 10–90%, open square represents mean. Analysis of statistical significance at the 0.05 level was determined using one-way repeated measures ANOVA with Dunnett's correction relative to the basal (–60 to 0) time-frame post hoc. To evaluate the effect of RapR-Shp2 versus FRB control two-way repeated measures ANOVA with Holm-Bonferroni correction was performed for pairwise analysis of each time point for RapR-Shp2 and FRB control. * $P < 0.05$, ** $P < 0.01$, *** $P < 0.001$.

Implementation of RapR allosteric switches in other protein tyrosine phosphatases

We aimed to demonstrate the broad applicability of this approach for regulation of PTPs. Using sequence and structural homology, we identified potential sites for insertion of iFKBP in tyrosine phosphatases PTP1B and PTP-PEST (Fig. 10 A). As with RapR-Shp2, we evaluated flexible linkers of varying lengths to optimize regulation of each of these PTPs. The shortest flexible linker, a single Gly, disrupted phosphatase activity with and without rapamycin for both PTP1B and PTP-PEST (Fig. 10, B–E). Increasing the length of the flexible linker to GPG resulted in improved dynamic range of regulation for both PTP1B and PTP-PEST (Fig. 10, B–E). In both PTPs, this linker promoted disruption of phosphatase activity in the absence of rapamycin and recovery of activity with the addition of rapamycin. RapR-PTP1B and RapR-PTP-PEST with the longest linker showed dramatically reduced dynamic range of regulation (Fig. 10, B–E). These results demonstrate the broad applicability of this approach in regulation of protein tyrosine phosphatases as well as the tunability of this regulation through the modification of the flexible linkers.

Discussion

We developed a temporally regulated tool to study Shp2 signaling on a physiologically relevant time scale. The RapR-Shp2 tool utilizes a highly dynamic allosteric switch in the Shp2 catalytic domain to disrupt catalytic activity and recover activity following the addition of FRB and rapamycin (Fig. 3, B and C). Furthermore, we validated that insertion of the iFKBP domain does not disrupt canonical functions of Shp2. RapR-Shp2 induced ERK activity, recognized and dephosphorylated established Shp2 substrates, and formed previously described protein-protein interactions mediated by SH2 domains (Fig. 4). We also demonstrated the general applicability of this approach to other PTPs (Fig. 10, B and C). Other tools developed to study phosphatases, such as an optogenetically controlled PTP1B developed by Hongdusit et al. (2020), possess many of the same advantages of our tools but lack facile implementation in a variety of PTPs and the capability to reconstruct individual downstream pathways (Hongdusit et al., 2020). We also described an approach for optimization of the tool by varying insertion site flexibility, thus providing a template for the future design of allosterically regulated tools.

The importance of Shp2 in cell migration, polarization, and protrusions has been repeatedly established (Cao et al., 2019; Grosskopf et al., 2015; Hartman et al., 2013; Hu et al., 2014; Lee et al., 2013; Sausgruber et al., 2015; Zhang et al., 2015). However, due to the limitations of the tools, the timing, extent, and sequence of events specifically induced by Shp2 activation has not been fully determined. We overcome the limitations of conventional molecular biology approaches to demonstrate that acute Shp2 activation can recapitulate known Shp2 signaling and morphological changes with added temporal and spatial resolution. Using RapR-Shp2, we provided direct evidence that Shp2 activity induces cell spreading, protrusions, and migration even in the absence of parallel signaling pathways induced by growth factor stimulation (Fig. 5, A–E). These dynamic behaviors showed dependency on the duration of Shp2 signaling, with an initial increase in cell spreading and protrusions, delayed initiation of retraction, and transient induction of migration. These transient events could not be detected using CA-Shp2 in HeLa cells. Our results show the importance of a temporally regulated tool to study the intricacies of Shp2 signaling on a physiologically relevant time scale.

Previous reports suggested that increased Shp2 activity leading to hyperphosphorylation of ERK contributes to migratory phenotypes, and that ERK activity stabilizes protrusions at the leading edge of a cell (Mendoza et al., 2015; Mizutani et al., 2007). We found that in the absence of MEK/ERK signaling, Shp2 still induces moderate cell migration but not sustained cell spreading (Fig. 6, A–C). Using specific SH2 domain mutants to selectively block phospho-tyrosine binding by each SH2 domain, we observed that protein-protein interactions mediated by the N-SH2 domain of Shp2 are sufficient to induce ERK-independent cell migration (Fig. 7 D). Further, our data suggest that this ERK-independent migration is mediated through Shp2-regulated ROCK II activity (Fig. 7 D), revealing multiple Shp2-dependent pathways for the induction of cell migration.

Unexpectedly, Shp2 regulation of cell retraction was unaffected by MAPK or ROCK II inhibition (Fig. 6 D and Fig. 7 E). Only the loss of the N-SH2 domain binding resulted in a reduction of cell retraction (Fig. 7 E). This suggests an additional Shp2 signaling pathway responsible for driving cell contraction, likely mediated through interaction with the N-SH2 domain. The specific and temporal regulatory capabilities of the RapR-Shp2 tool provide a unique opportunity to further dissect these pathways to better understand Shp2-mediated morphological changes.

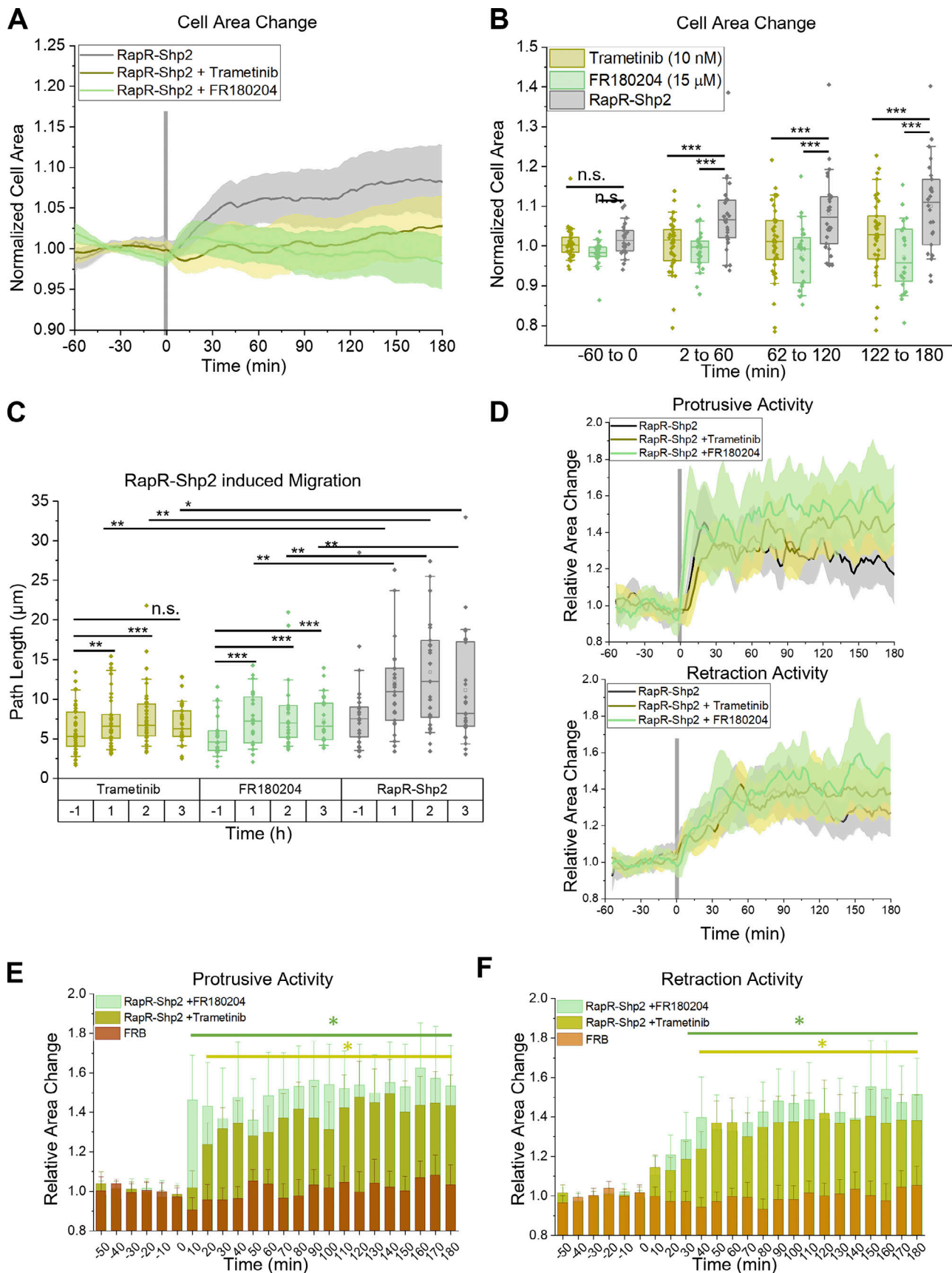


Figure 6. **Role of ERK activation in mediating RapR-Shp2-induced changes in cell morphology.** HeLa cells transiently coexpressing RapR-Shp2-mVenus-flag and mCherry-ipep-FRB were stained with CellMask Deep Red membrane marker and treated with 10 nM Trametinib ($N = 39$ cells, four separate biological

replicates) or 15 μ M FR180204 ERK1/2 inhibitor ($N = 24$ cells, three independent biological replicates) for 1 h prior to imaging. Rapamycin was added at 0 min (gray line in A and D). CellMask Deep Red images were used for analysis. Data for RapR-Shp2 from Fig. 4 included for comparison (gray). **(A and B)** Analysis of changes in cell area for trametinib (mustard) or FR180204 (mint) treated cells. (A) Shaded area represents 90% CI. (B) Box and whisker plots of relative cell area change binned over 1 h intervals for FR180204-treated cells (mint, $F[3,1] = 0.48$, $P = 0.700$) and for Trametinib-treated cells (mustard, $F[3,1] = 1.88$, $P = 0.138$). Both inhibitors cause significant reduction in cell spreading versus RapR-Shp2: Trametinib ($F[3,1] = 10.79$, $P < 0.001$), FR180204 ($F[3,1] = 8.30$, $P < 0.001$). **(C)** Changes in cell migration (determined as path length over 1 h intervals) for FR180204-treated cells (mint, $F[3,1] = 10.68$, $P < 0.001$) and for Trametinib-treated cells (mustard, $F[3,1] = 6.05$, $P < 0.001$). **(D–F)** Analysis of the protrusive and retraction activity (D) for trametinib (mustard), FR180204 (mint), and nontreated cells (data from Fig. 4, B and D in gray). Shaded area represents 90% CI. (E and F) Bar graph of Protrusive (E) and Retraction (F) activity binned over 10 min intervals. Error bars show 90% CI. (E) There were significant differences in protrusive activity means for FR180204-treated cells (mint, $F[23,1] = 9.53$, $P < 0.001$) at time points 10–180 min and for Trametinib-treated cells (mustard, $F[23,1] = 10.91$, $P < 0.001$) at time points 20–180 min. (F) There were significant differences in retraction activity means for FR180204-treated cells (mint, $F[23,1] = 12.39$, $P < 0.001$) at time points 30–180 min and for Trametinib-treated cells (mustard, $F[23,1] = 14.33$, $P < 0.001$) at time points 40–180 min. (B, C, E, and F) Analysis of statistical significance at the 0.05 level was determined using one-way repeated measures ANOVA with Dunnett's correction relative to the basal (–60 to 0 min, –1 h, or 0 min) time-frame post hoc. (B and C) Box and whisker plots: Box indicates first through third quartile with median line, whiskers are 10–90%, open square represents mean. To evaluate the effect of RapR-Shp2 versus each inhibitor two-way repeated measures ANOVA with Holm-Bonferroni correction was performed for pairwise analysis of each time point for RapR-Shp2 and each inhibitor. * $P < 0.05$, ** $P < 0.01$, *** $P < 0.001$.

In addition, we used RapRTAP to probe the importance of Shp2 signaling within specific protein complexes. We identified morphological changes caused by different Shp2 signaling complexes: those mediated by Gab1 or Gab2 scaffolding proteins and focal adhesion protein complexes. Targeted activation of RapR-Shp2 in complex with Gab1/2 demonstrated transient cell migration with robust protrusive and retractive activity (Fig. 8, D and E). This morphology may potentially be mediated by Shp2-Gab-dependent activation of Src family kinases (Ren et al., 2004). Activation of this pathway was effective at stimulating necessary pathways for migration, but a loss of direct Shp2 activity in focal adhesions likely prevented the formation of nascent focal adhesions and local signaling. Hence, Gab targeting only partially reconstructed Shp2-mediated morphological changes.

In contrast, targeted activation of Shp2 within focal adhesions induced transient spreading and protrusions in an ERK-dependent manner (Fig. 8, B–D and Fig. S5 B). While we demonstrated the necessity of ERK activity in this transient spreading event, it remains to be seen if this is due to local pools of active ERK within focal adhesions. Notably, R32L RapR-Shp2 activation within focal adhesions is incapable of inducing cell retraction or migration. This suggests a possible loss of signaling required for migration which could be, in part, due to an inability to induce polarized contractility mediated by ROCK II. Shp2-mediated migration and protrusions can be reconstituted, potentially through ROCK II, in combination with cell spreading by targeting R138L RapR-Shp2 to focal adhesions (Fig. 9). Application of RapRTAP-Shp2 tool will enable the identification of specific players mediating these alternative pathways in future studies.

In summary, we presented a protein engineering tool that enables allosteric regulation of protein tyrosine phosphatases. This method provides high specificity and tight temporal control of phosphatase activation. We demonstrated that this approach allows us to mimic Shp2 signaling in living cells revealing transient effects of Shp2 activation and parallel signaling pathways mediating cell spreading and migration. Targeting activation of the engineered phosphatase to a specific protein complex allowed us to reconstruct individual signaling pathways downstream of Shp2 and determine their role in regulation of cell morphodynamics. Thus, this approach will provide a

powerful tool for dissection of physiological and pathological functions of tyrosine phosphatases.

Materials and methods

Antibodies, reagents, and cell lines

The following antibodies were used: anti-FLAG (cat. no. F3165; Millipore-Sigma, mouse), anti-FLAG (cat. no. MAB8529; Cell Signaling, mouse), anti-mCherry (cat. no. M11217; Invitrogen, rabbit), anti-GFP (cat. no. 632381; Clontech, mouse), anti-Myc (cat. no. 05-724; Millipore-Sigma, mouse), anti-paxillin (cat. no. BDB612405; Thermo Fisher Scientific, mouse), anti-phospho-paxillin (Tyr¹¹⁸; cat. no. 44-722G; Invitrogen, mouse), anti-p44/42 (ERK1/2; cat. no. 9102; Cell Signaling, rabbit), anti-p44/42 (ERK1/2; Thr²⁰²/Tyr²⁰⁴; cat. no. 9101; Cell Signaling, rabbit), anti-EGFR (cat. no. 2232; Cell Signaling, rabbit), anti-phospho-EGFR (Tyr⁹⁹²; cat. no. 2235; Cell Signaling, rabbit), anti-FAK (cat. no. 06-543; Millipore-Sigma, mouse), anti-phospho-FAK (Tyr^{576/577}; cat. no. 3281; Cell Signaling, rabbit), anti-PLC γ (cat. no. 5690; Cell Signaling, rabbit), and anti-phospho-PLC γ (Tyr⁷⁸³; cat. no. 14008; Cell Signaling, rabbit), anti-Gab1 (cat. no. 3232; Cell Signaling, rabbit), anti-phospho-Gab1 (Tyr⁶²⁷; cat. no. 3231; Cell Signaling, rabbit), anti-phospho-Gab1 (Tyr⁶⁵⁹; cat. no. 12745; Cell Signaling, rabbit), anti-ROCK II (cat. no. 8236; Cell Signaling, rabbit), anti-phospho-ROCK II (Tyr⁷²²; cat. no. SAB4301564; Sigma-Aldrich, rabbit), anti-phospho-MLC 2 (Ser¹⁹/Thr¹⁸; cat. no. 3674; Cell Signaling, rabbit), and anti-Shp2 (cat. no. 3397; Cell Signaling, rabbit).

The following cell lines were used: HeLa cells (cat. no. CCL-2; ATCC), human embryonic kidney HEK293T cells (cat. no. CRL-3216; ATCC), HEK293FT (cat. no. R70007; Thermo Fisher Scientific), and A431 epidermoid carcinoma cells (cat. no. CRL-1555; ATCC). All cell lines were cultured at 37°C and 5% carbon dioxide in DMEM medium supplemented with 10% vol/vol fetal bovine serum and 1% vol/vol GlutaMAX. All experiments were performed with cells grown for <20 passages after thawing. All cells were tested negative for *Mycoplasma* contamination. Cell line identity was confirmed by the supplier using STR analysis. DH5 α bacteria cells (cat. no. C2987H; NEB) were used for GST-paxillinN-C3 production.

The following reagents were used: IgG-coupled agarose beads (cat. no. IP04-1.5ML; Millipore-Sigma), Leupeptin hemisulfate (cat. no. L-010-5; Gold Biotechnology), Aprotinin (cat. no.

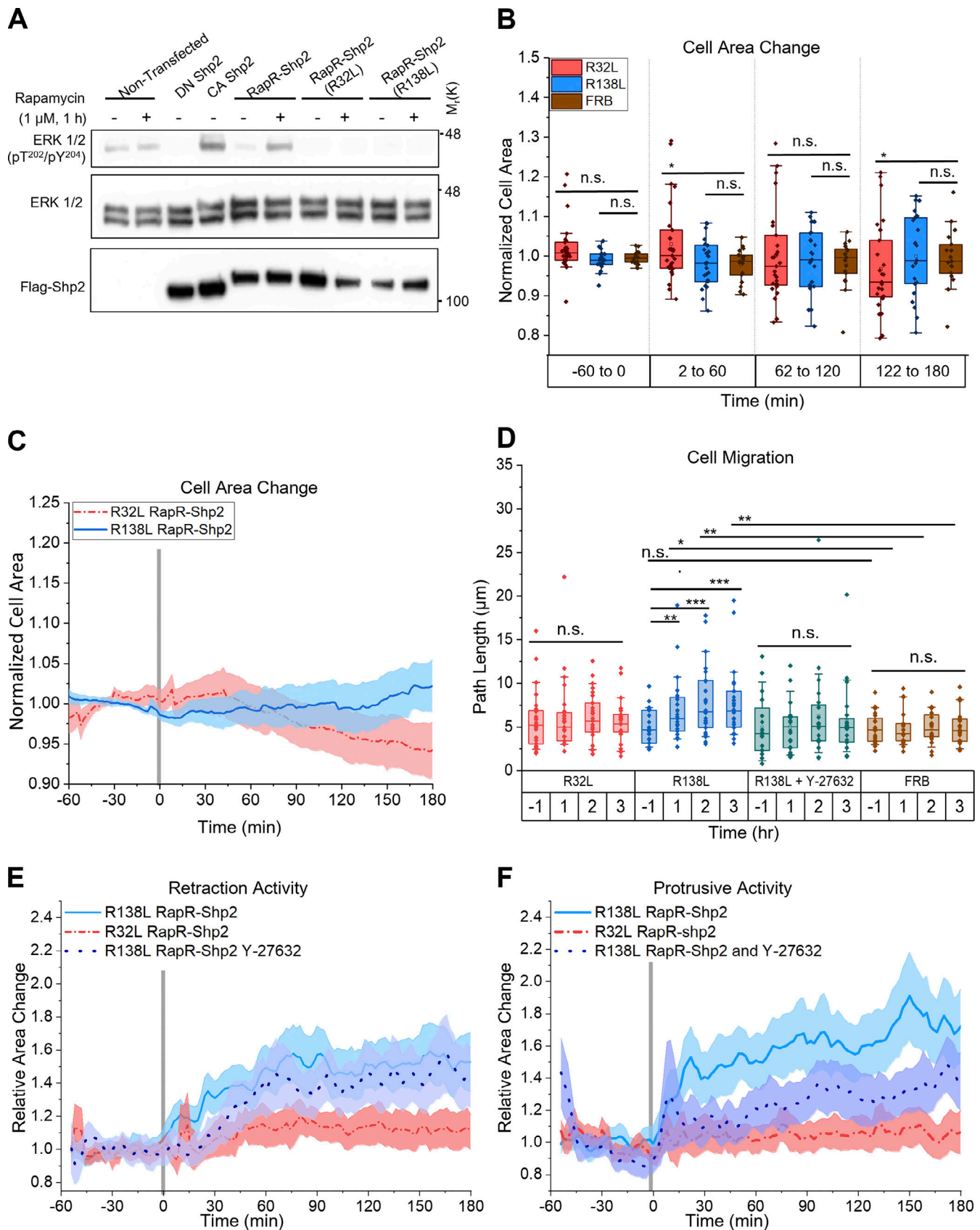


Figure 7. **Role of N-SH2 domain of Shp2 in mediating ERK-independent migration and protrusive activity through a parallel ROCK II pathway.** (A) Activation of ERK by Shp2 signaling. HEK293T cells transiently coexpressing indicated constructs and mCherry-FRB were treated with rapamycin for 1 h and cell lysates were analyzed by immunoblotting. A representative blot of $N = 4$ independent experiments is shown. (B-F) HeLa cells transiently expressing R32L

($N = 27$ cells, four separate biological replicates) or R138L ($N = 23$ cells, four separate biological replicates) mutants of RapR-Shp2-Cerulean-flag and mVenus-ipep-FRB were stained with CellMask Deep Red membrane marker and imaged live. Rapamycin was added at 0 min (gray line in C, E, and F). (B) Normalized area of cells expressing R32L (red, $F[3,1] = 2.97$, $P = 0.083$), R138L (blue, $F[3,1] = 0.66$, $P = 0.57$), or FRB alone (brown, data from Fig. 5) binned over 1 h intervals. Pairwise comparison of R32L or R138L vs FRB: R32L ($F[3,1] = 6.40$, $P < 0.001$), R138L ($F[3,1] = 0.24$, $P = 0.87$) (C) Changes in cell area in response to R32L (red, dashed line) or R138L (blue, solid line) RapR-Shp2 activation. Shaded area represents 90% CI. (D) Path length of cell centroid over 1 h intervals for R32L (red, $F[3,1] = 0.52$, $P = 0.670$) or R138L (blue, $F[3,1] = 10.43$, $P < 0.001$) RapR-Shp2, FRB control (brown, Data from Fig. 4) or R138L RapR-Shp2 pretreated with 10 μ M Y-27632 (ROCK II inhibitor, $N = 20$ cells, three separate biological replicates) for 1 h (teal, $F[3,1] = 1.07$, $P = 0.370$). Only R138L RapR-Shp2 exhibited a significant effect vs FRB: R32L ($F[3,1] = 0.77$, $P = 0.51$), R138L ($F[3,1] = 5.92$, $P = 0.001$), R138L + Y-27632 ($F[3,1] = 0.78$, $P = 0.51$). (E and F) Changes in Protrusive Activity (E) and Retraction activity (F) of analyzed in C. Shaded area represents 90% CI. (B and D) Box and whisker plots: Box indicates first through third quartile with median line, whiskers are 10–90%, open square represents mean. Analysis of statistical significance at the 0.05 level was determined using one-way repeated measures ANOVA with Dunnett's correction relative to the basal (–60 to 0 min or –1 h) time-frame post hoc. To evaluate the effect of each RapR-Shp2 SH2 domain mutant vs FRB two-way repeated measures ANOVA with Holm-Bonferroni correction was performed for pairwise analysis of each time point. * $P < 0.05$, ** $P < 0.01$, *** $P < 0.001$.

A-655-25; Gold Biotechnology), Y-27632 dihydrochloride (cat. no. Y0503; Millipore-Sigma), 2X Laemmli Sample buffer (cat. no. 161-0737; Bio-Rad), 2-Mercaptoethanol (cat. no. 60-24-2; Fisher Chemical), trypsin (cat. no. V5113; Promega), Fetal Bovine Serum (cat. no. FB-01; Omega Scientific), and CellMask Deep Red Plasma Membrane Stain (cat. no. C10046; Thermo Fisher Scientific), GlutaMAX (cat. no. 35050061; Thermo Fisher Scientific). Coverslips for live imaging were purchased from Thermo Fisher Scientific (cat. no. 25CIR-1.5).

Molecular biology and expression plasmids

Dominant Negative Shp2-flag and Constitutively Active Shp2-flag plasmids were a gift from the Graeme Carnegie lab (UIC). PTP1B and PTP-PEST were a gift from Nicholas Tonks (Cold Spring Harbor Laboratory). iFKBP was inserted at the designated insertion sites in CA-Shp2, WT-PTP1B, and PTP-PEST using a modified site-directed mutagenesis method as described by Karginov et al. (2010). An mVenus or Cerulean fluorescent tag was inserted at the C-terminus of Shp2. R32L and R138L point mutations were introduced using site-directed mutagenesis. FRB-GFP-Gab1 and FRB-GFP-Gab2 were developed from Gab1 and Gab2 plasmids which were a gift from Benjamin Neel (NYU). FRB was inserted in pGFP-c1 vector using the modified site-directed mutagenesis method with using an FRB megaprimer. Gab1 and Gab2 genes were amplified using primers generating XhoI and BamHI restriction sites at the ends of the genes. These restriction sites were used to insert Gab1 or Gab2 into the FRB-GFP vector. Y/F mutations were then introduced within both of these constructs at Tyr⁶²⁸/Tyr⁶⁶⁰ in Gab1 and Tyr⁶⁰⁴/Tyr⁶³⁴ in Gab2 using site-directed mutagenesis. To generate FAK (Y397) FRB-mVenus, FRB was inserted in FAK-mVenus using modified site-directed mutagenesis, replacing the Tyr³⁹⁷ site with FRB. Venus-ipep-FRB and mCherry-ipep-FRB and adenoviral mCherry-FRB as described by Klomp et al. (2019) were used. LeGO-iV2 was a gift from Boris Fehse (plasmid # 27344; Addgene; <http://n2t.net/addgene:27344>; RRID:Addgene_27344; Weber et al., 2008), pMD2.G was a gift from Didier Trono (plasmid # 12259; Addgene; <http://n2t.net/addgene:12259>; RRID:Addgene_12259), psPAX2 was a gift from Didier Trono (plasmid # 12260; Addgene; <http://n2t.net/addgene:12260>; RRID:Addgene_12260), GST-paxillinN-C3 construct was a gift from Michael Schaller (Lyons et al., 2001). In order to prepare lentiviral RapR-Shp2, RapR-Shp2-mVenus-flag was PCR amplified with primers to introduce NotI and BsiWI on the 5'- and -3'

ends. The PCR product, along with Lego-iV2 plasmid, was digested with NotI and BsrGI then ligated with generate lentiviral Lego-iV2 RapR-Shp2-mVenus-flag.

Primers

iFKBP insertion at V406 single glycine linker in Shp2 mega primer
 5'-CTATACGCTAAGAGAAGCTTAACTTTCAAAGGGTACCTGCGTGGTGCCTACACCGGGATGCTTGAAGATGGAAGAAATTGATTCCCTCCCGGGACAGAAACAAGCCCTTTAAGTTTATGCTAGGCAAGCAGGAGGTGATCCGAGGCTGGGAAGAAGGGTTGCCAGATGAGTGTGGTCCAGAGAGCCAACTGACTATATCTCCAGATTATGCCTATGGTGCCACTGGGCACCCAGGCATCATCCCACCACATGCCACTCTCGTCTTCGATGTGGAGCTTCTAAAAGTGGGAAGGACAAGGAATACGGAGAGAACGGTCTGGC-3'.

Addition of GSG linker at V406 in RapR-Shp2

Forward: 5'-TTTACGAGAGCTCAAAGCTCTCTAAAGTCGGCTCTGGTGGTACCTGCGTGGTGCCTACAC-3'.

Reverse: 3'-GACGGTTCTCTCTGTGTTCCCTGGCCACCAGAGCCCTCCAGTTTTAGAAGCTCCACAT-5'.

Forward: 5'-TACACTTACGAGAGCTCAAAGCTCTCAGGAAGCGGTACCTGCGTGGTGCCTACACCG-3'.

Reverse: 3'-CTGCCAGACGGTCTCTCTGTGTTCCCGAAGCGCCTCCAGTTTTAGAAGCTCCAC-5'.

Deletion of K405 in RapR-Shp2

Forward: 5'-CCGCCATGACTACACTTTACGAGAG-3'.

Reverse: 3'-GAAAGTGGTACTGCCAGACGGTTCTCT-5'.

Deletion of G407 in RapR-Shp2

Forward: 5'-GCCCATGACTACACTTTACGAGAGCTCAAAGCTCTCAGGTACCTGCGTGGTGCCTACACCG-3'.

Reverse: 3'-AAAGTGGTACTGCCAGACGGTCTCTCTGTGTTACCGCCTCCAGTTTTAGAAGCTCCAC-5'.

iFKBP insertion at K317 in Shp2 mega primer

5'-GCAAATATCATCATGCCTGAATTTGAAACCGGTACCTGCGTGGTGCCTACACCGGGATGCTTGAAGATGGAAGAAATTTGATTCCCTCCCGGGACAGAAACAAGCCCTTTAAGTTTATGCTAGGCAAGCAGGAGGTGATCCGAGGCTGGGAAGAAGGGTTGCCAGATGAGTGTGGTCCAGAGAGCCAACTGACTATATCTCCA GATTATGCCTATGGTGCCACTGGGCACCCAGGCATCATCCCA CCACATGCCACTCTCGTCTTCGATGTGGAGCTTCTAAAAGTGGGAATCAAAGCCAAAAGAGTTACATTGCCACAC-3'.

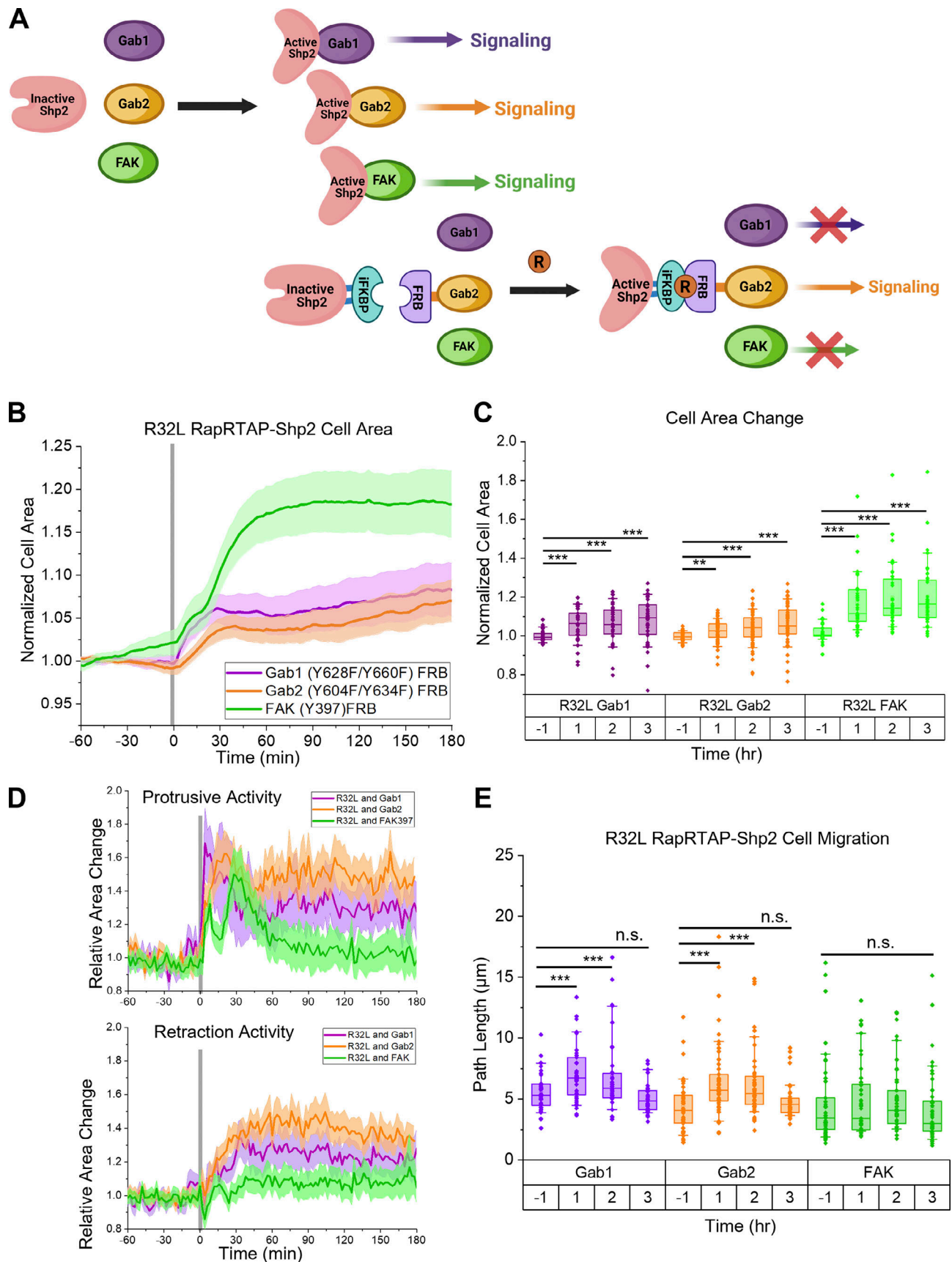


Figure 8. Regulation of cell spreading and migration by Shp2 activation in different signaling complexes. (A) Schematic of RapRTAP system to specifically target and activate different Shp2 signaling complexes. RapRTAP-Shp2 can be independently targeted to FRB-Gab1 (purple), FRB-Gab2 (orange) or

FAK-FRB (green). **(B–E)** HeLa cells transiently expressing R32L RapR-Shp2-Cerulean-flag and the FRB fused target protein were stained with CellMask Deep Red membrane dye and imaged live. Rapamycin was added at 0 min (gray line in B and D). CellMask images were used for analysis. (B and C) Changes in the area of cells coexpressing R32L RapR-Shp2 and FRB fusion proteins: FRB-GFP-Gab1 (Y628F/Y660F) ($N = 38$ cells, five separate biological replicates), FRB-GFP-Gab2 (Y604F/Y634F) ($N = 57$ cells, five separate biological replicates), and FAK-FRB-mVenus ($N = 43$ cells, four separate biological replicates). (C) Changes in cell area (over 1 h intervals) induced by activation of Shp2 targeted to Gab1 (purple, $F[3,1] = 16.69$, $P < 0.001$), Gab2 (orange, $F[3,1] = 17.05$, $P < 0.001$), and FAK (green, $F[3,1] = 67.18$, $P < 0.001$). (D) Changes in Protrusive and Retraction activity induced by R32L RapR-Shp2 targeted to Gab1 (purple), Gab2 (orange), and FAK (green). (E) Changes in cell migration (shown as path length over 1 h intervals) induced by activation of Shp2 targeted to Gab1 (purple, $F[3,1] = 19.68$, $P < 0.001$), Gab2 (orange, $F[3,1] = 23.03$, $P < 0.001$), and FAK (green, $F[3,1] = 2.63$, $P = 0.053$). (C and E) Box and whisker plots: Box indicates first through third quartile with median line, whiskers are 10–90%, open square represents mean. Analysis of statistical significance at the 0.05 level was determined using one-way repeated measures ANOVA with Dunnett's correction post hoc relative to basal (–1 h). * $P < 0.05$, ** $P < 0.01$, *** $P < 0.001$.

iFKBP insertion at T288 in Shp2 mega primer

5'-TAGATATAAAAAACATCCTGCCCTTTGATCATGGTACCTGCGT
GGTGCCTACACCGGGATGCTTGAAGATGGAAGAAATTTGA
TTCTCCCGGGACAGAAACAAGCCCTTTAAGTTTATGCTAGG
CAAGCAGGAGGTGATCCGAGGCTGGGAAGAAGGGTTGCCCA
GATGAGTGTGGTCCAGAGAGCCAACTGACTATATCTCCAGA
TTATGCCTATGGTGCCACTGGGCACCCAGGCATCATCCACC
ACATGCCACTCTCGTCTTCGATGTGGAGCTTCTAAAAGTGA
AAGGGTTGCTTACACGATGGTATCCCAATGAG-3'.

iFKBP insertion in PTP1B mega primer

5'-CAGTGCACAGCTAGAATTGGAAAACGGTACCTGCGTGG
TGCCTACACCGGGATGCTTGAAGATGGAAGAAATTTGATT
CCTCCCGGGACAGAAACAAGCCCTTTAAGTTTATGCTAGGCA
AGCAGGAGGTGATCCGAGGCTGGGAAGAAGGGTTGCCAGA
TGAGTGTGGTCCAGAGAGCCAACTGACTATATCTCCAGATT
ATGCCTATGGTGCCACTGGGCACCCAGGCATCATCCACCAC
ATGCCACTCTCGTCTTCGATGTGGAGCTTCTAAAAGTGAAG
GTCAAAGGAGTTACATTCTTACCAGGGC-3'.

iFKBP insertion in PTP-Pest mega primer

5'-GACTACTTCATCAGGACACTCTTACTTGAATTCGGACCAGGT
ACCTGCGTGGTGCCTACACCGGGATGCTTGAAGATGGAAG
AAATTTGATTCTCCCGGGACAGAAACAAGCCCTTTAAGTTT
ATGCTAGGCAAGCAGGAGGTGATCCGAGGCTGGGAAGAAGGG
GTTGCCAGATGAGTGTGGTCCAGAGAGCCAACTGACTATA
TCTCCAGATTATGCCATGCTGCTTTCGATGTGGAGCTTCTA
AACTGGAAGTCCCGGACAAAATGAATCTCGTAGGCTGTAT
CAGTTTCATTA-3'.

R32L in Shp2

Forward: 5'-GAGGAGTCGATGGCAGTTTTTTAGCAC-3'.
Reverse: 3'-GAAGTCTCCAGGGTTACTCTTACTGGG-5'.

R318L in Shp2

Forward: 5'-GGCAAGCATGGCAGCTTCTCGTTCTA-5'.
Reverse: 3'-GAGAACGAAGTCTCCGGGGTGGCTCT-3'.

Insertion of FRB in pGFP-C1 vector mega primer

5'-CGAGCGGCCGCACTGTGCTGGATCATGGCTTCTAGAATCCT
CTGGCATGAGATGTGGCATGAAGGCTGGAAGAGGCATCTCG
TTTGTACTTTGGGAAAAGGAACGTGAAAGGCATGTTGAGGT
GCTGGAGCCCTTGCATGCTATGATGGAACGGGGCCCCAGAC
TCTGAAGGAAACATCCTTTAATCAGGCCTATGGTTCGAGATTT
AATGGAGGCCAAGAGTGGTGCAGGAAGTACATGAAATCAGG

GAATGTCAAGGACCTCCTCCAAGCCTGGGACCTCTATTATCA
TGTGTTCCGACGAATCTCAAAGACTAGTGGTGGCAGTGGAAAC
CAGCAAGGGCGAGGAGCTGTTACCG-3'.

Cloning of Gab1 into FRB-GFP vector

Forward: 5'-GATACTCTCGAGGTATGAGCGGCGGGAAGTGG
TTTG-3'.
Reverse: 3'-GACACCCACCAAGAATGTGAAGTGAGGATCCCA
TAAG-5'.

Y628F in Gab1

Forward: 5'-GAATAAACCCAAAGGAGACAAACAAGTCGAATT
CCTGGATTTAGACCTAGATTCTGGGA-3'.
Reverse: 3'-TCCCAGAATCTAGGTCTAAATCCAGGAATTCGA
CTTGTCTCTCTTTGGGT-5'.

Y660F in Gab1

Forward: 5'-GCAGCATGGCAGACGAGAGGGTGGATTTCTGTTG
TGGTGGACCAACAGAAGACTC-3'.
Reverse: 3'-GAGTCTTCTGTTGGTCCACCACAACGAAATCCA
CCCTCTCGTCTGCCATGCTGC-5'.

Cloning of Gab2 into FRB-GFP vector

Forward: 5'-GATACTCTCGAGGTATGAGCGGCGGCGGCGGGC
ACG-3'.
Reverse: 3'-GAACCTTCCAAGGGTGCCAAGCTGTAAGGATCC
CACGAC-5'.

Y604F in Gab2

Forward: 5'-CAAAGAAGAGTACTGGCAGTGTGGATTTTCTCG
CCCTGGACTTCCAGCCGGGCTC-3'.
Reverse: 3'-GAGCCCGGCTGGAAGTCCAGGGCGGAGAAAATCC
ACACTGCCAGTACTCTTCTTTG-5'.

Y634F in Gab2

Forward: 5'-CTGTCACATCAGATGAGAAGGTAGACTTTGTCC
AAGTGGATAAAGAGAAGACCC-3'.
Reverse: 3'-GGGTCTTCTTTTATCCACTTGGACAAAAGTCTA
CCTTCTCATCTGATGTGACAG-5'.

FRB insertion at Y397 in FAK mega primer

5'-CATGCAGTCTCTGTGTCAGAGACAGATGACGGCCCCGGA
TGGCATGAGATGTGGCATGAAGGCTGGAAGAGGCATCTCGT
TTGTACTTTGGGAAAAGGAACGTGAAAGGCATGTTGAGGTG
CTGGAGCCCTTGCATGCTATGATGGAACGGGGCCCCAGACT
CTGAAGGAAACATCCTTTAATCAGGCCTATGGTTCGAGATTTA

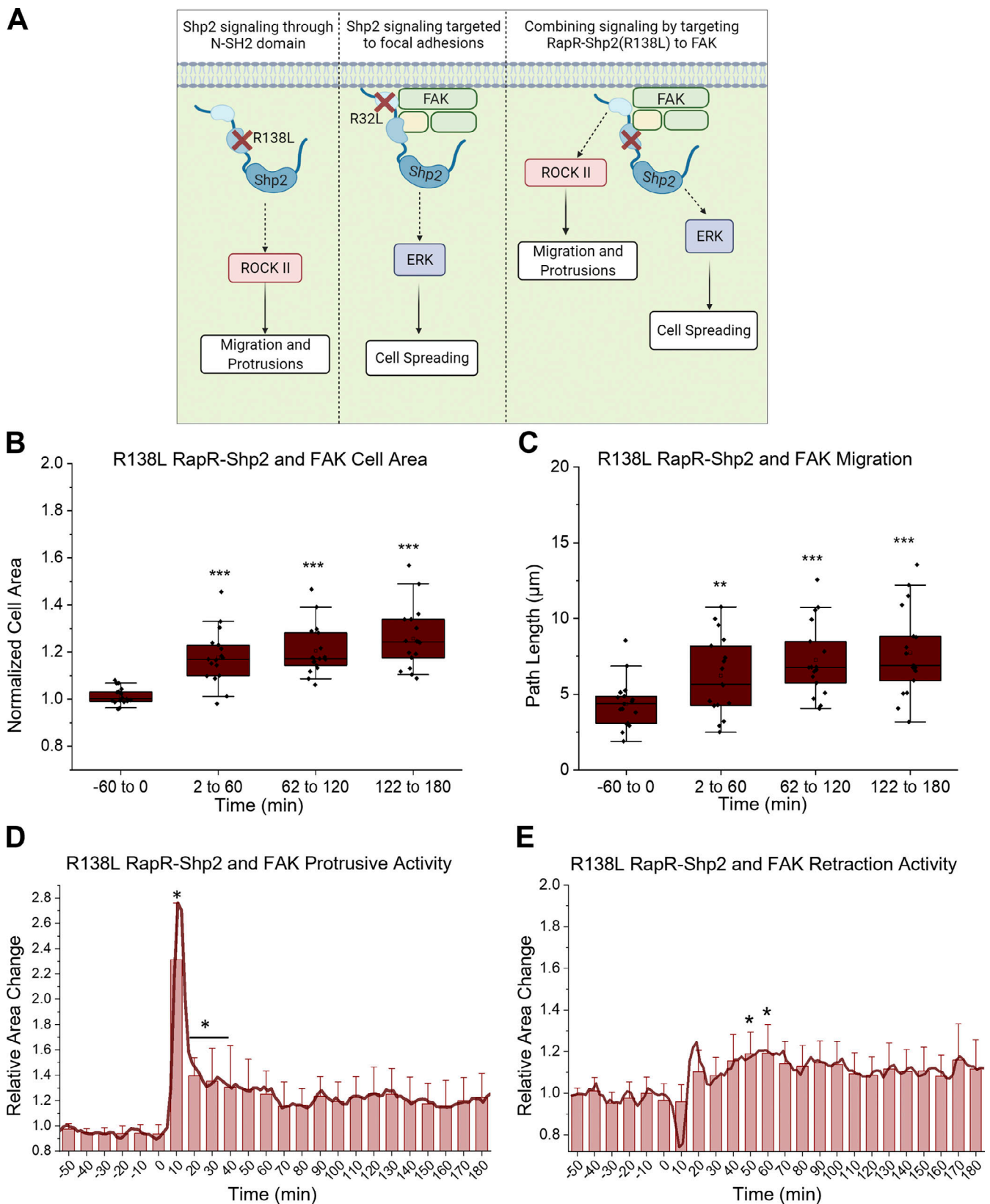


Figure 9. **Combining parallel Shp2-mediated pathways to reconstruct cell morphodynamics.** (A) Schematic representation of individual signaling pathways mediated by N-SH2 domain of Shp2 and Shp2 signaling in focal adhesions. Protein-protein interactions mediated by the N-SH2 domain of Shp2 are sufficient to induce ROCK II-dependent cell migration following activation of Shp2 (Left). Shp2 activation in focal adhesion complexes results in downstream activation of ERK and ERK dependent spreading in the absence of N-SH2-mediated protein-protein interactions (Middle). Combined signaling through local Shp2 activation in focal adhesion complexes and N-SH2 domain-mediated protein-protein interactions reconstitutes both cell spreading and cell migration

(right). (B–E) Created with biorender.com. HeLa cells transiently expressing R138L RapR-Shp2-Cerulean-flag and FAK(397)FRB-mVenus were stained with CellMask Deep Red membrane dye and imaged live. CellMask images were used for analysis. $N = 17$ cells, three independent experiments. (B) Changes in cell area induced by activation of R138L RapR-Shp2 in focal adhesion complexes binned over 1 h intervals ($F[3,1] = 51.08$, $P < 0.001$). (C) Changes in cell migration shown as path length over 1 h intervals ($F[3,1] = 14.21$, $P < 0.001$). (D and E) Effect of R138L RapR-Shp2 activation in focal adhesion complexes on Protrusive (D) and Retraction (E) activity binned over 10 min intervals with mean activity at each 2 min timepoint overlaid as a solid line, error bars show 90% CI. Activation of R138 L RapR-Shp2 in complex with FAK induced significant changes in protrusion ($F[23,1] = 10.10$, $P < 0.001$) from time points 10–40 min and significant changes in retraction ($F[23,1] = 2.53$, $P < 0.001$) from time point 50–60 min. (B–E) Analysis of statistical significance at the 0.05 level was determined using one-way repeated measures ANOVA with Dunnett's correction relative to the basal (–60 to 0, or 0 min) time-frame post hoc. (B and C) Box and whisker plots: Box indicates first through third quartile with median line, whiskers are 10–90%, open square represents mean.

ATGGAGGCCCAAGAGTGGTGCAGGAAGTACATGAAATCAGGG
AATGTCAAGGACCTCCTCCAAGCCTGGGACCTCTATTATCAT
GTGTTCCGACGAATCTCAAAGACTAGTGACCCGGTGCAGAG
ATCATCGATGAGGAAGACACATAC-3'.

NotI and BsiWI introduction at Shp2-mVenus-flag 5' - and -3'

Forward: 5'-ATCGTACTGCGGCCGCATGACATCGCGGAGATG
GTTTCACC-3'.

Reverse: 3'-TGCTACGATCGTACGTCACTTGTCTGCATCGTC
CTTGTAGT-5'.

Transient expression in HEK293T cells and ERK activation assay

For expression of the RapR phosphatase constructs and FRB constructs, HEK293T cells were grown to 70% confluency on a plastic dish coated with 1:200 poly-L-lysine and were transfected with Lipofectamine 2000. A transfection solution of 500 μ l of Opti-MEM, 4 μ l Lipofectamine 2000, and 2 μ g of DNA was added to the cells and incubated overnight. Cells were stimulated with 1 μ M Rapamycin in ethanol for 1 h or listed time points for the time course of ERK activation assay. Control cells were treated with an equivalent volume of ethanol. Cells were then lysed in 2X Laemmli sample buffer with 5% 2-mercaptoethanol, and proteins were resolved via sodium dodecyl sulfate-polyacrylimide gel electrophoresis (SDS/PAGE) and immunoblotted. Blots were developed using enhanced chemiluminescence.

Preparation of phosphorylated paxillin

An N-terminal fragment of paxillin was purified using a previously described procedure (Lyons et al., 2001). The GST-paxillin-N-C3 construct was expressed in DH5 α *E. coli* cells following inductions with 0.1 mM Isopropyl β -D-1-thiogalactopyranoside for 4 h. The bacterial pellet was resuspended in 30 ml of TETN buffer (20 mM TRIS pH 8, 10 mM NaCl, 1 mM EDTA, 0.5% [vol/vol] Triton X-100) then lysed by sonication. Using affinity chromatography with Glutathione Sepharose, GST-tagged paxillin was purified from the cleared lysates.

The purified GST-paxillin was then phosphorylated using an immunoprecipitated constitutively active c-Src. HEK293FT cells 70% confluent in a 10-cm dish were transfected with c-Src (Y527F)-mCherry. Cells were lysed with lysis buffer (20 mM HEPES-KOH, pH 7.8, 50 mM KCl, 1 mM EGTA, 1% NP-40, aprotinin 16 μ g/ml, and Leupeptin hemisulfate 3.2 μ g/ml). Lysates were cleared through centrifugation at 2683 RCF for 10 min at 4°C. Protein G Agarose beads were preincubated with anti-myc antibody (4A6 from Millipore-Sigma) for 1 h at 4°C.

Cleared lysates were incubated with anti-myc conjugated beads for 1.5 h at 4°C. Beads were then washed twice with wash buffer (20 mM Hepes-KOH, pH 7.8, 100 mM NaCl, 50 mM KCl, 1 mM EGTA, 1% NP-40) and then with kinase reaction buffer (25 mM HEPES, pH 7.5, 5 M MgCl₂, 0.5 mM EGTA, 0.005% BRIJ-35). The beads were resuspended in kinase reaction buffer and incubated with 0.1 mM ATP and 0.05 mg/ml purified N-terminal fragment of paxillin (GST-paxillinN-C3) at 37°C for 10 min. The reaction buffer containing the phosphorylated paxillin fragment was then separated from the Agarose beads conjugated with c-Src(Y527F)-mCherry via centrifugation. Phosphorylation of paxillin was verified with SDS/PAGE and immunoblotting for paxillin phosphorylation.

In vitro phosphatase activity assays

HEK293T cells coexpressing the RapR Phosphatase constructs and mVenus-ipep-FRB or mCherry-ipep-FRB (Klomp et al., 2019) were treated with 1 μ M Rapamycin for 1 h prior to lysis (Lyons et al., 2001). Cells were lysed in a HEPES sample buffer (20 mM HEPES-KOH pH 7.8, 50 mM KCl, 1 mM EGTA, and 1% NP-40 [vol/vol]). Lysates were cleared via centrifugation at 2683 g RCF for 10 min at 4°C. Protein G Agarose beads were preincubated with anti-FLAG or anti-GFP antibody (F3165; Sigma-Aldrich) for 1 h in lysis buffer. Lysates were incubated with anti-FLAG or anti-GFP conjugated beads at 4°C for 1.5 h. Following incubation, beads were washed twice with 1 ml of lysis buffer and twice with 1 ml of wash buffer (20 mM HEPES-KOH, pH 7.8, 100 mM NaCl, 50 mM KCl, 1 mM EGTA, 1% NP-40 [vol/vol]). Beads were resuspended in 40 μ l Imidazole reaction buffer (25 mM Imidazole pH 7.2, 2.5 mM EDTA, 50 mM NaCl, 5 mM DTT) containing purified phosphorylated N-terminal fragment of paxillin. The immunoprecipitated RapR phosphatases were then incubated with purified phosphorylated paxillin for 30 min, or for the specified times in the time course of CA-Shp2 and RapR-Shp2 phosphatase activity, at 32°C. The reaction was quenched with the addition of 2X Laemmli sample buffer with 5% (vol/vol) 2-mercaptoethanol and boiling at 100°C for 5 min. Proteins were resolved via SDS/PAGE and immunoblotted.

Relative kinetic values, K_m and V_{max} , were determined using the approach described by Orsi and Tipton (1979) for substrate depletion over time. Briefly, plotting ($[\text{Substrate}_0] - [\text{Substrate}_t]$)/time vs. ($\ln([\text{Substrate}_t]/[\text{Substrate}_0])$)/t, we generated a linear graph with a slope of $-K_m$ and a y-intercept of V_{max} . Using immunoblot intensity, we established the zero time point for both CA-Shp2 and RapR-Shp2 as 1.0 and evaluated the disappearance of substrate through the change in relative blot

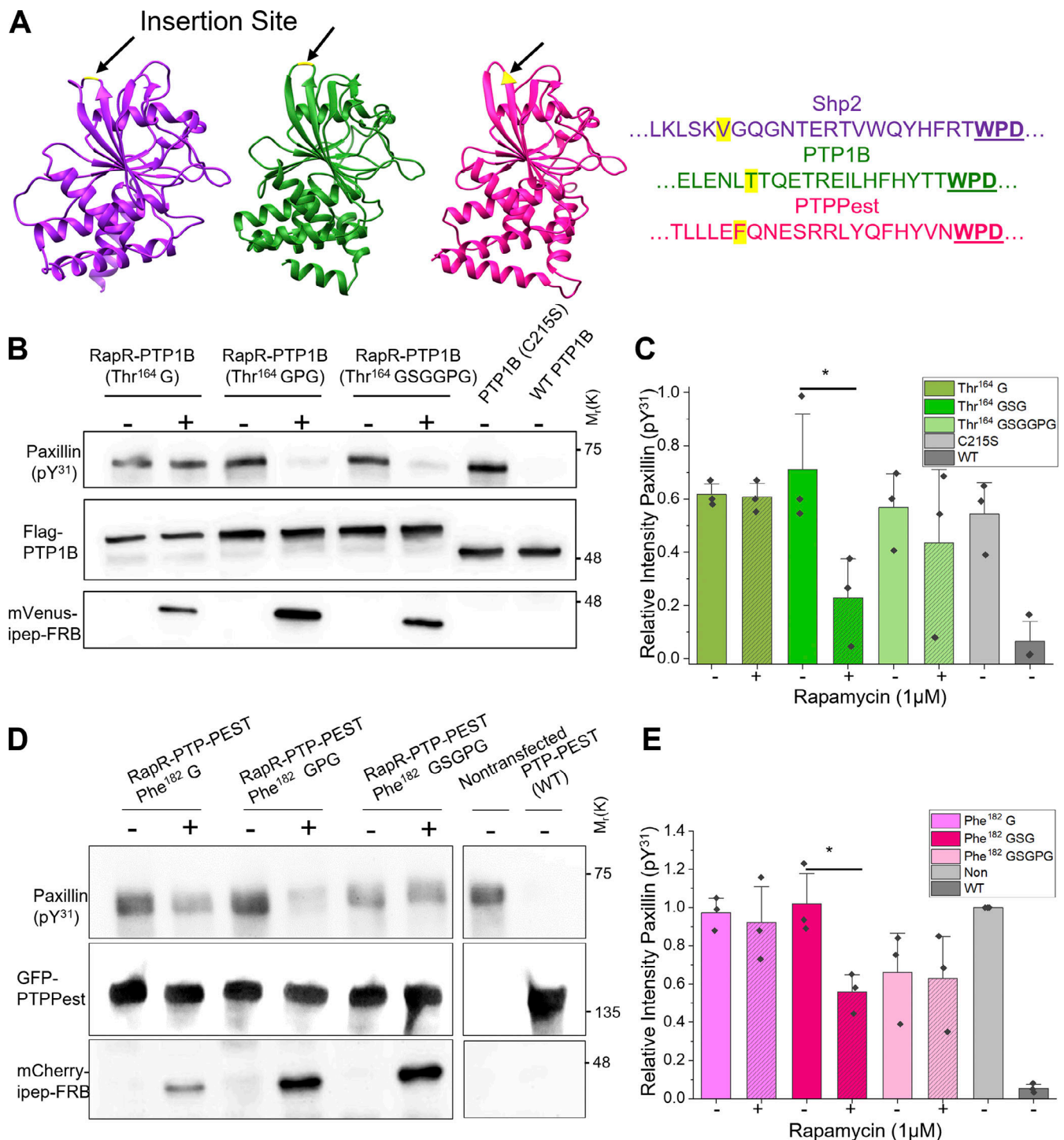


Figure 10. **Implementation of Engineered Allosteric regulation in PTP1B and PTP-PEST.** (A) Depiction of Shp2 (purple), PTP1B (green), and PTP-PEST (magenta) with the homologous insertion sites to Val⁴⁰⁶ in Shp2 highlighted in yellow (arrows). (right) Amino acid sequences of the regions adjacent to the insertion site in Shp2, PTP1B, and PTP-PEST (catalytically important WPD loop is bolded). (B–E) Cell-free in vitro assay evaluating phosphatase activity. Indicated PTP1B-flag and PTP-PEST-GFP constructs were coexpressed with mVenus-ipep-FRB (B and C) or mCherry-ipep-FRB (D and E) in HEK293 cells, activated with rapamycin, immunoprecipitated and incubated with phosphorylated paxillin for 30 min. (B and C) Analysis of activity for wild-type PTP1B-flag (WT PTP1B), dominant negative PTP1B (PTP1B[C215S]), and three linker variations (G, GPG, or GPGGSG) of RapR-PTP1B with iFKBP inserted at Thr¹⁶⁴. (C) Analysis of activity for wild-type PTP-PEST (PTP-PEST WT), three linker variations (G, GPG, or GPGGSG) of RapR-PTP-PEST-GFP with iFKBP inserted at Phe¹⁸², and nontransfected control immunoprecipitated using anti-GFP antibody. Representative blots of *N* = 3 independent experiments shown with quantification (C and E). Error bars show 90% CI. Analysis of statistical significance at the 0.05 level was determined by two-tailed Student's *t* test for independent pairwise comparisons of each linker with and without rapamycin. **P* < 0.05.

intensity. This value was used as a proxy for substrate concentration to evaluate the relative kinetic values for CA-Shp2 and RapR-Shp2 and the differences in K_m and V_{max} . CA-Shp2 relative kinetic values: $K_m = 0.85$ R.I. and $V_{max} = -0.012$ R.I./min. RapR-Shp2 relative kinetic values: $K_m = 1.04$ R.I. and $V_{max} = -0.026$ R.I./min. Thus, RapR-Shp2 shows 1.2-fold increase in K_m and 2.2-fold increase in V_{max} over corresponding values for CA-Shp2.

Lentivirus preparation and transduction

Lego-iV2-RapR-Shp2-mVenus-flag was cotransfected with lentiviral envelope protein VSV-G in pMD2.G plasmid and a second-generation lentiviral packaging plasmid, psPAX2 in HEK293T cells. Conditioned media were collected 1–3 d after transfection, and the virus was concentrated using Lenti-X concentrator following the manufacturer's protocol. A431 cells were then grown to 80% confluency and transduced using the concentrated virus.

Assessment of RapR-Shp2 activation in A431 cells

A431 cells were transduced with lentiviral RapR-Shp2-mVenus-flag and mCherry-FRB adenovirus. Confluent stably expressing A431 cells were serum starved for 4 h prior to stimulation with 1 μ M rapamycin for 2 and 4 h. Samples without rapamycin were treated with an equivalent volume of ethanol for 4 h. Non-expressing A431 cells were treated either with rapamycin or with an equivalent volume of ethanol as controls.

Coimmunoprecipitation

A431 cells were transduced with lentiviral RapR-Shp2-mVenus and mCherry-FRB adenovirus, lentiviral CA-Shp2-mVenus, or mCherry-FRB adenovirus. Confluent, stably expressing, A431 cells were activated with 1 μ M rapamycin for 2 h. Protein G Plus Agarose (IPO4; Sigma) beads were preincubated with anti-GFP antibody for 1 h in lysis buffer. Samples were lysed with HEPES sample buffer (20 mM HEPES-KOH pH 7.8, 50 mM KCl, 1 mM EGTA, and 1% NP-40 [vol/vol]) and centrifuged at 12,000 rpm for 10 min. Lysate was incubated with anti-GFP conjugated Protein G Plus beads for 1.5 h at 4°C. Following incubation, beads were washed twice with 1 ml of lysis buffer and twice with 1 ml of wash buffer (20 mM HEPES-KOH, pH 7.8, 250 mM NaCl, 50 mM KCl, 1 mM EGTA, 1% NP-40 [vol/vol]). Proteins were eluted with Laemmli sample buffer and resolved via SDS/PAGE and immunoblotting.

Live cell imaging and analysis

HeLa cells were grown to 60% confluency in a 35-mm dish and transfected with 6 μ l of Fugene6 and 1 μ g of total DNA and incubated overnight. These cells were seeded at 30% confluency on fibronectin-coated (5 mg/l) glass coverslips for 4 h prior to imaging and serum starved in Leibovitz L-15 imaging media for 2 h prior to imaging. All cells were stained with CellMask Deep Red plasma membrane stain (cat. no. C10046; Thermo Fisher Scientific) prior to imaging following manufacturer's recommendation. Using epifluorescence imaging, we selected cells coexpressing all necessary constructs. Cells were imaged live at 37°C in an open heated chamber (Werner Instruments) using

Olympus UPlanSAPO 40 \times (oil, N.A. 1.25) objective on Olympus IX-83 microscope controlled by Metamorph software and equipped with Xcite 120 LED (Lumen Dynamics) light source and Image EMX2 CCD camera (Hamamatsu). Time lapse images were acquired every 2 min over the duration of the imaging experiment, 4–4.5 h. In the experiments using Trametinib, cells were treated with 10 nM Trametinib for 1 h prior to imaging. HeLa cells used for the ROCK II inhibition studies were treated with 10 μ M Y-27632 dichloride (cat. no. Y0503; Millipore-Sigma) for 1 h prior to imaging.

Epifluorescence images of CellMask Deep Red were used to analyze changes in cell morphology. The binary mask of the images was created using MovThresh 2014 (Tsygankov et al., 2014) software package in Matlab (version 2017a). Cell area, in pixels, was calculated in ImageJ for each timepoint. In order to determine the area change for each cell, the area at each time point was normalized to the average area of the cell in the time prior to stimulation with rapamycin. The average of these normalized values and 90% confidence interval were then calculated for all cells for each condition.

To analyze the changes in protrusive activity of the cells, the binary masks described above were analyzed using ProActive2014 script in Matlab (version 2017a; Tsygankov et al., 2014). Total cell area was used to normalize the area gained and lost, with a lag of one frame. The protrusive and retractive area for each time point was divided by the average of the protrusive or retractive area prior to rapamycin addition. The average and 90% confidence interval for the relative protrusive and retractive area were again calculated for all cells in each condition.

Analysis of cell migration was determined using ImageJ software. The centroid of the cell was determined for each time point. The distance traveled over each 2-min time point was calculated and the total path length was determined for 1-h intervals.

Plots for all imaging analyses were generated in OriginPro 2019.

In silico analysis of RapR-Shp2

In silico analysis of RapR-Shp2 was performed using NAMD v2.13 software (Phillips et al., 2020). Models of RapR-Shp2 were created using PDB accession no. 4DGP for Shp2 catalytic domain and PDB accession no. 4FAP for the FKBP-Rapamycin-FRB complex. The unresolved loops within the catalytic domain of Shp2 (residues 295–301 and 314–323) were created and refined using Modeller (Šali and Blundell, 1993). Insertion of iFKBP in Shp2 to generate these models was performed as previously described (Karginov et al., 2010). All simulations were conducted in explicit solvent at 310 K. Models were minimized and equilibrated prior to conducting a 50-ns MD simulation. All models were simulated in three independent runs with slightly different starting structures to increase the conformational space sampled. The first 10 ns of each run were discarded for analysis.

Statistics

All in vitro data, imaging data, and Western blots are representative of at least three independent experiments. Western

blots were quantified using ImageJ software. Error bars in plots are representative of a confidence interval of 90%. Box and whisker plots: Box indicates first through third quartile with median line, whiskers are 10–90%, open square represents mean. Significance was determined using ANOVA with appropriate post hoc analysis or two-tailed Student's *t* test. Data distribution was assumed to be normal but this was not formally tested.

All in vitro phosphatase assays were analyzed using two-tailed Student's *t* test. This test was selected to enable pairwise comparisons of each modification with and without rapamycin to evaluate statistically significant induction of phosphatase activity by each individual construct.

One-way ANOVA with Holm-Bonferroni post hoc analysis was used for comparison of multiple related means. This was applied to evaluate the influence of the RapR insertion on activation of ERK relative to a catalytically dead and constitutively active Shp2 or evaluate inhibitor effects on ERK or MLC phosphorylation.

Time courses an imaging data were evaluated using one-way ANOVA with repeated measures and post hoc Dunnett test to compare all time points to the zero point. Pairwise comparisons of multiple conditions at different time points, as with MAPK inhibition or comparison to controls, were performed using two-way ANOVA with repeated measures with post hoc Holm-Bonferroni pairwise comparisons between factors.

Online supplemental material

[Fig. S1](#) provides quantitative analysis of Western blots from [Fig. 3](#) as well as shows relative expression of RapR-Shp2 to endogenous Shp2. [Fig. S2](#) analyzes the protrusive and retraction activity of RapR-Shp2 expressing cells and the effects of CA-Shp2 on cell morphology. [Video 1](#) shows the cell mask movie of RapR-Shp2 expressing HeLa cells before and after activation. [Fig. S3](#) analyzes the influence of Shp2 SH2 domains on ERK activation and protrusive and retractive area as well as the effects of ROCK II and ERK inhibitors on SH2 domain-mediated cell morphology. [Fig. S4](#) shows the effects of RapRTAP Shp2 signaling complexes on cell protrusion and retraction as well as construct localization. [Video 2](#) shows the cell mask movie of R32L RapR-Shp2 and FRB-GFP-Gab1 (Y628F/Y660F) expressing HeLa cells before and after activation. [Video 3](#) shows the cell mask movie of R32L RapR-Shp2 and FRB-GFP-Gab2 (Y604F/Y634F) expressing HeLa cells before and after activation. [Video 4](#) shows the cell mask movie of R32L RapR-Shp2 and FAK(397)FRB-mVenus expressing HeLa cells before and after activation. [Fig. S5](#) demonstrates the effect of Shp2 activity within focal adhesions on ERK activity and cell spreading. [Video 5](#) shows the cell mask movie of R138L RapR-Shp2 and FAK(397)FRB-mVenus expressing HeLa cells before and after activation.

Acknowledgments

The authors would like to thank Dr. Martin Brennan and Dr. Mark Shaaya for technical assistance and discussion and Dr. Benjamin Neel for discussion and advice.

National Institute of Health-NIGMS grant R01GM118582 (A.V. Karginov), National Institute of Health-NCI grant R21CA212907

(A.V. Karginov), National Institute of Health T32 Training grant HL007829-22 (J. Fauser), US Department of Energy, Office of Science DE-AC02-06CH11357 (Y. Alexeev).

The authors declare no competing financial interests.

Author contributions: Investigation: J. Fauser, V. Huyot, J. Matsche, P. Kota. Validation: J. Fauser, V. Huyot, J. Matsche, B.N. Szynal. Methodology: J. Fauser, V. Huyot, P. Kota. Formal Analysis: J. Fauser, P. Kota. Visualization: J. Fauser. Funding acquisition: A.V. Karginov. Resources: Y. Alexeev. Supervision: A.V. Karginov. Conceptualization: A.V. Karginov. Project Administration: A.V. Karginov. Writing—original draft: J. Fauser. Writing—review and editing: J. Fauser, A.V. Karginov, P. Kota, B.N. Szynal, Y. Alexeev.

Submitted: 17 November 2021

Revised: 6 May 2022

Accepted: 22 June 2022

References

- Agazie, Y.M., and M.J. Hayman. 2003. Molecular mechanism for a role of SHP2 in epidermal growth factor receptor signaling. *Mol. Cell. Biol.* 23: 7875–7886. <https://doi.org/10.1128/MCB.23.21.7875-7886.2003>
- Anselmi, M., and J.S. Hub. 2020. An allosteric interaction controls the activation mechanism of SHP2 tyrosine phosphatase. *Sci. Rep.* 10:18530. <https://doi.org/10.1038/s41598-020-75409-7>
- Anselmi, M., P. Calligari, J.S. Hub, M. Tartaglia, G. Bocchinfuso, and L. Stella. 2020. Structural determinants of phosphopeptide binding to the N-terminal Src homology 2 domain of the SHP2 phosphatase. *J. Chem. Inf. Model.* 60:3157–3171. <https://doi.org/10.1021/acs.jcim.0c00307>
- Barua, D., J.R. Faeder, and J.M. Haugh. 2007. Structure-Based kinetic models of modular signaling protein function: Focus on Shp2. *Biophys. J.* 92: 2290–2300. <https://doi.org/10.1529/biophysj.106.093484>
- Neel, B.G., P. Lily, and L. Pao. 2003. The “Shp”ing news: SH2 domain-containing tyrosine phosphatases in cell signaling. *Trends Biochem. Sci.* 28:284–293. [https://doi.org/10.1016/S0968-0004\(03\)00091-4](https://doi.org/10.1016/S0968-0004(03)00091-4)
- Benjamin, G. G.C. Neel, D. Salim. 2010. SH2 domain containing protein-tyrosine phosphatases. In *Handbook of Cell Signaling*. Academic Press. San Diego. 771–809.
- Cao, M., D. Gao, N. Zhang, Y. Duan, Y. Wang, H. Mujtaba, and Y. Wang. 2019. Shp2 expression is upregulated in cervical cancer, and Shp2 contributes to cell growth and migration and reduces sensitivity to cisplatin in cervical cancer cells. *Pathol. Res. Pract.* 215:152621. <https://doi.org/10.1016/j.prp.2019.152621>
- Chichger, H., J. Braza, H. Duong, and E.O. Harrington. 2015. SH2 domain-containing protein tyrosine phosphatase 2 and focal adhesion kinase protein interactions regulate pulmonary endothelium barrier function. *Am. J. Respir. Cell Mol. Biol.* 52:695–707. <https://doi.org/10.1165/rcmb.2013-0489OC>
- Chu, P.-H., D. Tsygankov, M.E. Berginski, O. Dagliyan, S.M. Gomez, T.C. Elston, A.V. Karginov, and K.M. Hahn. 2014. Engineered kinase activation reveals unique morphodynamic phenotypes and associated trafficking for Src family isoforms. *Proc. Natl. Acad. Sci. USA.* 111:12420–12425. <https://doi.org/10.1073/pnas.1404487111>
- Cunnick, J.M., L. Mei, C.A. Doupnik, and J. Wu. 2001. Phosphotyrosines 627 and 659 of Gab1 constitute a bisphosphoryl tyrosine-based activation motif (BTAM) conferring binding and activation of SHP2. *J. Biol. Chem.* 276:24380–24387. <https://doi.org/10.1074/jbc.M010275200>
- Grosskopf, S., C. Eckert, C. Arkona, S. Radetzki, K. Böhm, U. Heinemann, G. Wolber, J.-P. Von Kries, W. Birchmeier, and J. Rademann. 2015. Selective inhibitors of the protein tyrosine phosphatase SHP2 block cellular motility and growth of cancer cells in vitro and in vivo. *ChemMedChem.* 10:815–826. <https://doi.org/10.1002/cmdc.201500015>
- Hartman, Z.R., M.D. Schaller, and Y.M. Agazie. 2013. The tyrosine phosphatase SHP2 regulates focal adhesion kinase to promote EGF-induced lamellipodia persistence and cell migration. *Mol. Cancer Res.* 11:651–664. <https://doi.org/10.1158/1541-7786.MCR-12-0578>
- Hartman, Z., W.J. Geldenhuys, and Y.M. Agazie. 2020. A specific amino acid context in EGFR and HER2 phosphorylation sites enables selective

- binding to the active site of Src homology phosphatase 2 (SHP2). *J. Biol. Chem.* 295:3563–3575. <https://doi.org/10.1074/jbc.RA119.011422>
- Hongdusit, A., P.H. Zwart, B. Sankaran, and J.M. Fox. 2020. Minimally disruptive optical control of protein tyrosine phosphatase 1B. *Nat. Commun.* 11:788. <https://doi.org/10.1038/s41467-020-14567-8>
- Hu, Z., H. Fang, X. Wang, D. Chen, Z. Chen, and S. Wang. 2014. Overexpression of SHP2 tyrosine phosphatase promotes the tumorigenesis of breast carcinoma. *Oncol. Rep.* 32:205–212. <https://doi.org/10.3892/or.2014.3201>
- Huang, Y.-S., C.-Y. Cheng, S.-H. Chueh, D.-Y. Hueng, Y.-F. Huang, C.-M. Chu, S.-T. Wu, M.-C. Tai, C.-M. Liang, M.-H. Liao, et al. 2012. Involvement of SHP2 in focal adhesion, migration and differentiation of neural stem cells. *Brain Dev.* 34:674–684. <https://doi.org/10.1016/j.braindev.2011.10.011>
- Karginov, A.V., F. Ding, P. Kota, N.V. Dokholyan, and K.M. Hahn. 2010. Engineered allosteric activation of kinases in living cells. *Nat. Biotechnol.* 28:743–747. <https://doi.org/10.1038/nbt.1639>
- Karginov, A.V., D. Tsygankov, M. Berginski, P.-H. Chu, E.D. Trudeau, J.J. Yi, S. Gomez, T.C. Elston, and K.M. Hahn. 2014. Dissecting motility signaling through activation of specific Src-effector complexes. *Nat. Chem. Biol.* 10:286–290. <https://doi.org/10.1038/nchembio.1477>
- Klomp, J.E., M. Shaaya, J. Matsche, R. Rebiai, J.S. Aaron, K.B. Collins, V. Huyot, A.M. Gonzalez, W.A. Muller, T.-L. Chew, et al. 2019. Time-variant SRC kinase activation determines endothelial permeability response. *Cell Chem. Biol.* 26:1081–1094.e6. <https://doi.org/10.1016/j.chembiol.2019.04.007>
- Lee, H.-H., and Z.-F. Chang. 2008. Regulation of RhoA-dependent ROCKII activation by Shp2. *J. Cell Biol.* 181:999–1012. <https://doi.org/10.1083/jcb.200710187>
- Lee, H.-H., H.-C. Lee, C.-C. Chou, S.S. Hur, K. Osterday, J.C. Del Alamo, J.C. Lasheras, and S. Chien. 2013. Shp2 plays a crucial role in cell structural orientation and force polarity in response to matrix rigidity. *Proc. Natl. Acad. Sci. USA.* 110:2840–2845. <https://doi.org/10.1073/pnas.1222164110>
- Liu, Y., B. Jenkins, J.L. Shin, and L.R. Rohrschneider. 2001. Scaffolding protein Gab2 mediates differentiation signaling downstream of Fms receptor tyrosine kinase. *Mol. Cell. Biol.* 21:3047–3056. <https://doi.org/10.1128/MCB.21.9.3047-3056.2001>
- Liu, W.-S., W.-Y. Jin, L. Zhou, X.-H. Lu, W.-Y. Li, Y. Ma, and R.-L. Wang. 2019. Structure based design of selective SHP2 inhibitors by De novo design, synthesis and biological evaluation. *J. Comput. Aided Mol. Des.* 33:759–774. <https://doi.org/10.1007/s10822-019-00213-z>
- Liu, Q., J. Qu, M. Zhao, Q. Xu, and Y. Sun. 2020. Targeting SHP2 as a promising strategy for cancer immunotherapy. *Pharmacol. Res.* 152:104595. <https://doi.org/10.1016/j.phrs.2019.104595>
- Lyons, P.D., J.M. Dunty, E.M. Schaefer, and M.D. Schaller. 2001. Inhibition of the catalytic activity of cell adhesion kinase β by protein-tyrosine phosphatase-PEST-mediated dephosphorylation. *J. Biol. Chem.* 276:24422–24431. <https://doi.org/10.1074/jbc.M011080200>
- Mañes, S., E. Mira, C. Gómez-Mouton, Z.J. Zhao, R.A. Lacalle, and C. Martínez-A. 1999. Concerted activity of tyrosine phosphatase SHP-2 and focal adhesion kinase in regulation of cell motility. *Mol. Cell. Biol.* 19:3125–3135. <https://doi.org/10.1128/MCB.19.4.3125>
- Matozaki, T., Y. Murata, Y. Saito, H. Okazawa, and H. Ohnishi. 2009. Protein tyrosine phosphatase SHP-2: A proto-oncogene product that promotes Ras activation. *Cancer Sci.* 100:1786–1793. <https://doi.org/10.1111/j.1349-7006.2009.01257.x>
- Mendoza, M.C., M. Vilela, J.E. Juarez, J. Blenis, and G. Danuser. 2015. ERK reinforces actin polymerization to power persistent edge protrusion during motility. *Sci. Signal.* 8:ra47. <https://doi.org/10.1126/scisignal.aaa8859>
- Meng, S., Z. Chen, T. Munoz-Antonia, and J. Wu. 2005. Participation of both Gab1 and Gab2 in the activation of the ERK/MAPK pathway by epidermal growth factor. *Biochem. J.* 391:143–151. <https://doi.org/10.1042/BJ20050229>
- Mizutani, K., H. Ito, I. Iwamoto, R. Morishita, T. Deguchi, Y. Nozawa, T. Asano, and K.-I. Nagata. 2007. Essential roles of ERK-mediated phosphorylation of vinexin in cell spreading, migration and anchorage-independent growth. *Oncogene.* 26:7122–7131. <https://doi.org/10.1038/sj.onc.1210512>
- Ogori, M., T. Kinoshita, M. Okubo, K. Sato, A. Yamazaki, H. Arakawa, S. Nishimura, N. Inamura, H. Nakajima, M. Neya, et al. 2005. Identification of a selective ERK inhibitor and structural determination of the inhibitor-ERK2 complex. *Biochem. Biophys. Res. Commun.* 336:357–363. <https://doi.org/10.1016/j.bbrc.2005.08.082>
- Orsi, B.A., and K.F. Tipton. 1979. Kinetic analysis of progress curves. *Methods Enzymol.* 63:159–183. [https://doi.org/10.1016/0076-6879\(79\)63010-0](https://doi.org/10.1016/0076-6879(79)63010-0)
- Paardekooper Overman, J., J.-S. Yi, M. Bonetti, M. Soulsby, C. Preisinger, M.P. Stokes, L. Hui, J.C. Silva, J. Overvoorde, P. Giansanti, et al. 2014. PZR coordinates Shp2 Noonan and LEOPARD syndrome signaling in Zebrafish and mice. *Mol. Cell Biol.* 34:2874–2889. <https://doi.org/10.1128/MCB.00135-14>
- Phillips, J.C., D.J.H. Phillips, J.D.C. Maia, J.E. Stone, J.V. Ribeiro, R.C. Bernardi, R. Buch, G. Fiorin, J. Hémin, W. Jiang, et al. 2020. Scalable molecular dynamics on CPU and GPU architectures with NAMD. *J. Chem. Phys.* 153:044130. <https://doi.org/10.1063/5.0014475>
- Qiu, W., X. Wang, V. Romanov, A. Hutchinson, A. Lin, M. Ruzanov, K.P. Battaile, E.F. Pai, B.G. Neel, and N.Y. Chirgadze. 2014. Structural insights into Noonan/LEOPARD syndrome-related mutants of protein-tyrosine phosphatase SHP2 (PTPN11). *BMC Struct. Biol.* 14:10. <https://doi.org/10.1186/1472-6807-14-10>
- Ran, H., R. Tsutsumi, T. Araki, and B.G. Neel. 2016. Sticking it to cancer with molecular glue for SHP2. *Cancer Cell.* 30:194–196. <https://doi.org/10.1016/j.ccell.2016.07.010>
- Ren, Y., S. Meng, L. Mei, Z.J. Zhao, R. Jove, and J. Wu. 2004. Roles of Gab1 and SHP2 in paxillin tyrosine dephosphorylation and Src activation in response to epidermal growth factor. *J. Biol. Chem.* 279:8497–8505. <https://doi.org/10.1074/jbc.M312575200>
- Ren, L., X. Chen, R. Luechapanichkul, N.G. Selner, T.M. Meyer, A.-S. Wavreille, R. Chan, C. Iorio, X. Zhou, B.G. Neel, and D. Pei. 2011. Substrate specificity of protein tyrosine phosphatases 1B, RPTPa, SHP-1, and SHP-2. *Biochemistry.* 50:2339–2356. <https://doi.org/10.1021/bi1014453>
- Lugowska, I., H. Koseła-Paterczyk, K. Kozak, and P. Rutkowski. 2015. Trametinib: A MEK inhibitor for management of metastatic melanoma. *Oncotargets Ther.* 8:2251–2259. <https://doi.org/10.2147/OTT.S72951>
- Šali, A., and T.L. Blundell. 1993. Comparative protein modelling by satisfaction of spatial restraints. *J. Mol. Biol.* 234:779–815. <https://doi.org/10.1006/jmbi.1993.1626>
- Sausgruber, N., M.-M. Coissieux, A. Britschgi, J. Wyckoff, N. Aceto, C. Leroy, M.B. Stadler, H. Voshol, D. Bonenfant, and M. Bentires-Alj. 2015. Tyrosine phosphatase SHP2 increases cell motility in triple-negative breast cancer through the activation of SRC-family kinases. *Oncogene.* 34:2272–2278. <https://doi.org/10.1038/onc.2014.170>
- Schaeper, U., N.H. Gehring, K.P. Fuchs, M. Sachs, B. Kempkes, and W. Birchmeier. 2000. Coupling of Gab1 to C-met, Grb2, and Shp2 mediates biological responses. *J. Cell Biol.* 149:1419–1432. <https://doi.org/10.1083/jcb.149.7.1419>
- Serra-Nedelec, A.D.R., T. Edouard, K. Treguer, M. Tajan, T. Araki, M. Dance, M. Mus, A. Montagner, M. Tauber, J.-P. Salles, et al. 2012. Noonan syndrome-causing SHP2 mutants inhibit insulin-like growth factor 1 release via growth hormone-induced ERK hyperactivation, which contributes to short stature. *Proc. Natl. Acad. Sci. USA.* 109:4257–4262. <https://doi.org/10.1073/pnas.1119803109>
- Sha, F., E.B. Gencer, S. Georgeon, A. Koide, N. Yasui, S. Koide, and O. Hantschel. 2013. Dissection of the BCR-ABL signaling network using highly specific monoclonal inhibitors to the SHP2 SH2 domains. *Proc. Natl. Acad. Sci. USA.* 110:14924–14929. <https://doi.org/10.1073/pnas.1303640110>
- Sun, J., S. Lu, M. Ouyang, L.-J. Lin, Y. Zhuo, B. Liu, S. Chien, B.G. Neel, and Y. Wang. 2013. Antagonism between binding site affinity and conformational dynamics tunes alternative cis-interactions within Shp2. *Nat. Commun.* 4:2037. <https://doi.org/10.1038/ncomms3037>
- Tajan, M., A. De Rocca Serra, P. Valet, T. Edouard, and A. Yart. 2015. SHP2 sails from physiology to pathology. *Eur. J. Med. Genet.* 58:509–525. <https://doi.org/10.1016/j.ejmg.2015.08.005>
- Tan, D., W. Zhang, Y. Tao, Y. Galiya, and M. Wang. 2019. PZR promotes metastasis of colorectal cancer through increasing FAK and Src phosphorylation. *Acta Biochim. Biophys. Sin.* 51:356–364. <https://doi.org/10.1093/abbs/gmz019>
- Tanimura, S., and K. Takeda. 2017. ERK signalling as a regulator of cell motility. *J. Biochem.* 162:145–154. <https://doi.org/10.1093/jb/mvx048>
- Tiganis, T., and A.M. Bennett. 2007. Protein tyrosine phosphatase function: The substrate perspective. *Biochem. J.* 402:1–15. <https://doi.org/10.1042/BJ20061548>
- Tonks, N.K. 2013. Protein tyrosine phosphatases: From housekeeping enzymes to master regulators of signal transduction. *FEBS J.* 280:346–378. <https://doi.org/10.1111/febs.12077>
- Tonks, N.K., and B.G. Neel. 2001. Combinatorial control of the specificity of protein tyrosine phosphatases. *Curr. Opin. Cell Biol.* 13:182–195. [https://doi.org/10.1016/s0955-0674\(00\)00196-4](https://doi.org/10.1016/s0955-0674(00)00196-4)
- Tsutsumi, R., A. Takahashi, T. Azuma, H. Higashi, and M. Hatakeyama. 2006. Focal adhesion kinase is a substrate and downstream effector of

- SHP-2 complexed with Helicobacter pylori CagA. *Mol. Cell Biol.* 26: 261–276. <https://doi.org/10.1128/MCB.26.1.261-276.2006>
- Tsygankov, D., C.G. Bilancia, E.A. Vitriol, K.M. Hahn, M. Peifer, and T.C. Elston. 2014. CellGeo: A computational platform for the analysis of shape changes in cells with complex geometries. *J. Cell Biol.* 204: 443–460. <https://doi.org/10.1083/jcb.201306067>
- Vazhappilly, C.G., E. Saleh, W. Ramadan, V. Menon, A.M. Al-Azawi, H. Tarazi, H. Abdu-Allah, A.-N. El-Shorbagi, and R. El-Awady. 2019. Inhibition of SHP2 by new compounds induces differential effects on RAS/RAF/ERK and PI3K/AKT pathways in different cancer cell types. *Invest. N. Drugs.* 37:252–261. <https://doi.org/10.1007/s10637-018-0626-5>
- Vidyasiri Vemulapalli, L.C., A. Erickson, J. LaRochelle, K. Subramanian, M. Mohseni, M. LaMarche, M.G. Acker, P.K. Sorger, S.P. Gygi, S.C. Blacklow. 2019. Time resolved quantitative phosphoproteomics reveals distinct patterns of SHP2 dependence in EGFR signaling. bioRxiv. (Preprint posted April 12, 2019). <https://doi.org/10.1101/598664>
- Guo, W., and Q. Xu. 2020. Phosphatase-independent functions of SHP2 and its regulation by small molecule compounds. *J. Pharmacol. Sci.* 144: 139–146. <https://doi.org/10.1016/j.jphs.2020.06.002>
- Weber, K., U. Bartsch, and B. Fehse. 2008. A multicolor panel of novel lentiviral “gene ontology” (LeGO) vectors for functional gene analysis. *Molecular Therapy.* 16:698–706. <https://doi.org/10.1038/mt.2008.6>
- Witsenburg, J.J., H. Glauner, J.P. Müller, J.M.M. Groenewoud, G. Roth, F.-D. Böhmer, M.J.W. Adjobo-Hermans, and R. Brock. 2013. A quantitative assessment of costimulation and phosphatase activity on microclusters in early T cell signaling. *PLoS One.* 8:e79277. <https://doi.org/10.1371/journal.pone.0079277>
- Wu, J.-C., Y.-C. Chen, C.-T. Kuo, H. Wenshin Yu, Y.-Q. Chen, A. Chiou, and J.-C. Kuo. 2015. Focal adhesion kinase-dependent focal adhesion recruitment of SH2 domains directs SRC into focal adhesions to regulate cell adhesion and migration. *Sci. Rep.* 5:18476. <https://doi.org/10.1038/srep18476>
- Xu, C., X. Wu, M. Lu, L. Tang, H. Yao, J. Wang, X. Ji, M. Hussain, J. Wu, and X. Wu. 2019. Protein tyrosine phosphatase 11 acts through RhoA/ROCK to regulate eosinophil accumulation in the allergic airway. *FASEB J.* 33: 11706–11720. <https://doi.org/10.1096/fj.201900698R>
- Yang, F., M. Xu, S. Wang, L. Song, D. Yu, Y. Li, R. Cao, Z. Xiong, Z. Chen, Q. Zhang, et al. 2019. Gain-Of-Function E76K-mutant SHP2 promotes cell proliferation, metastasis, and tumor growth in glioblastoma through activation of the ERK/CREB pathway. *Oncotargets Ther.* 12:9435–9447. <https://doi.org/10.2147/OTT.S222881>
- Yu, D.-H., C.-K. Qu, O. Henegariu, X. Lu, and G.-S. Feng. 1998. Protein-tyrosine phosphatase shp-2 regulates cell spreading, migration, and focal adhesion. *J. Biol. Chem.* 273:21125–21131. <https://doi.org/10.1074/jbc.273.33.21125>
- Yu, Z.-H., J. Xu, C.D. Walls, L. Chen, S. Zhang, R. Zhang, L. Wu, L. Wang, S. Liu, and Z.-Y. Zhang. 2013. Structural and mechanistic insights into LEOPARD syndrome-associated SHP2 mutations. *J. Biol. Chem.* 288: 10472–10482. <https://doi.org/10.1074/jbc.M113.450023>
- Zhang, X., G. Lavoie, L. Fort, E.L. Huttlin, J. Tcherkezian, J.A. Galan, H. Gu, S.P. Gygi, S. Carreno, and P.P. Roux. 2013. Gab2 phosphorylation by RSK inhibits Shp2 recruitment and cell motility. *Mol. Cell Biol.* 33: 1657–1670. <https://doi.org/10.1128/MCB.01353-12>
- Zhang, J., F. Zhang, and R. Niu. 2015. Functions of Shp2 in cancer. *J. Cell Mol. Med.* 19:2075–2083. <https://doi.org/10.1111/jcmm.12618>

Supplemental material

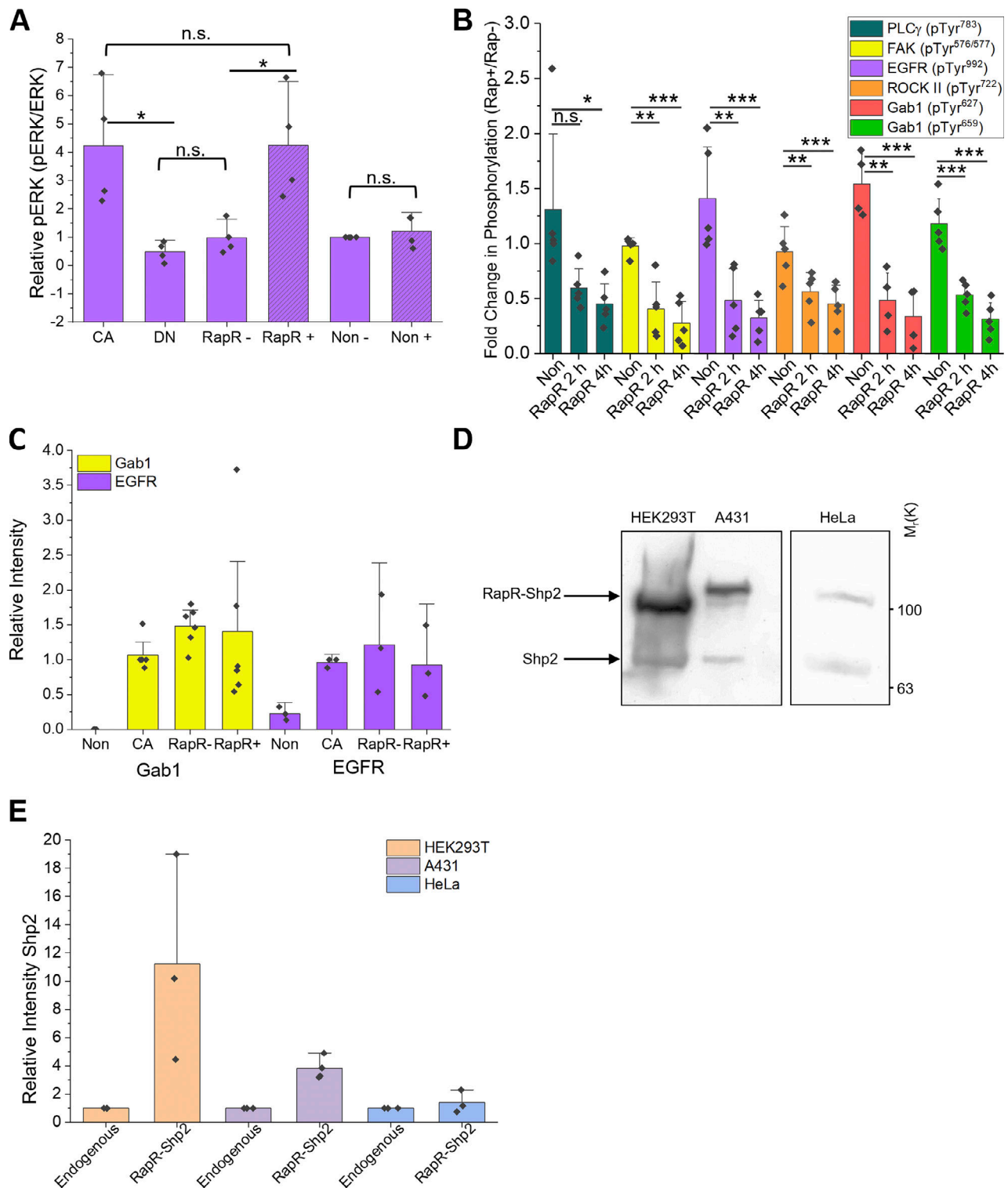


Figure S1. **Validation of RapR-Shp2 cellular function.** (A) Analysis of Western blot intensity for ERK activation following RapR-Shp2 activation (Fig. 3 A). All phospho-ERK (pT²⁰²/pY²⁰⁴) signals are normalized to total ERK blot intensity. One-way ANOVA analysis with post hoc Holm-Bonferroni test for pairwise comparison at a significance level of 0.05. ANOVA $F = 7.63$, $P = 0.001$. * $P < 0.05$. (B) Analysis of the signal intensity for EGFR (pY⁹⁹²) ($F[2,1] = 21.45$, $P < 0.001$), FAK (pY^{576/577}) ($F[2,1] = 25.35$, $P < 0.001$), PLCγ (pY⁷⁸³) ($F[2,1] = 4.56$, $P = 0.047$), ROCK II (pY⁷²²) ($F[2,1] = 26.23$, $P < 0.001$), Gab1 (pY⁶²⁷) ($F[2,1] = 30.87$, $P < 0.001$) or (pY⁶⁵⁹) ($F[2,1] = 42.49$, $P < 0.001$), normalized to corresponding total protein signal, following Rapamycin treatment for 2 or 4 h (Fig. 3 B). Each phosphorylation site was analyzed for significance at the 0.05 level using one-way repeated measures ANOVA with post hoc Dunnett's method to pairwise compare the fold-change in phosphorylation for each time point relative to the noninfected control group. * $P < 0.05$, ** $P < 0.01$, *** $P < 0.001$. (C) Analysis of coimmunoprecipitation of Gab1 and EGFR with FRB-mCherry (non), CA-Shp2-venus, and RapR-Shp2-venus shown in Fig. 4 C (normalized to Shp2). (D-E) Comparison of RapR-Shp2 and endogenous Shp2 expression levels in HEK293T, A431, and HeLa cells. Representative blot of $N = 3$ independent experiments with quantification (E). All error bars show 90% CI.

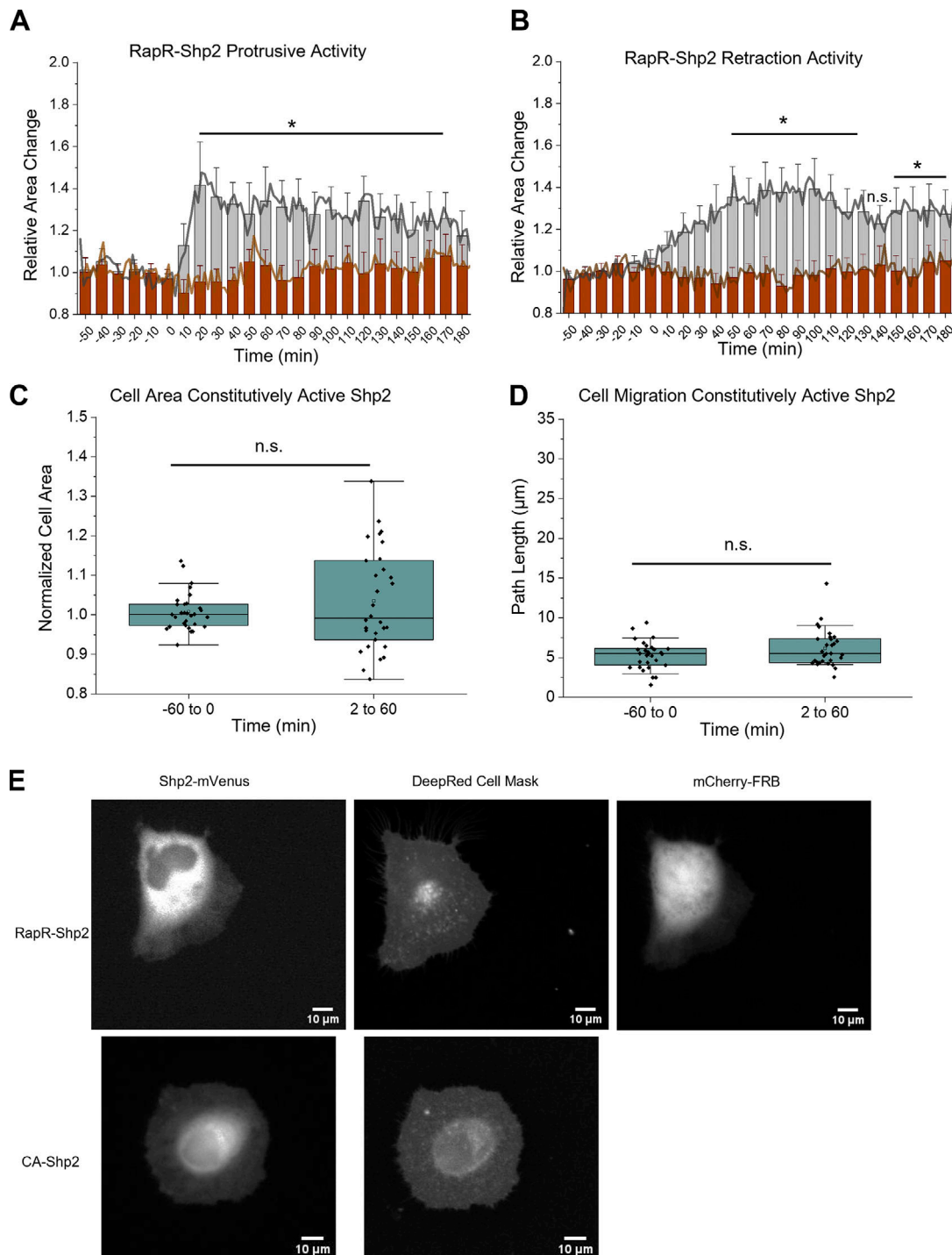


Figure S2. **Characterization of transient effects induced by Shp2 activation.** (A and B) Relative Protrusive (A) and Retractive (B) area changes for RapR-Shp2 (gray) and FRB (brown) expressing cells binned over 10 min intervals, mean activity at each 2 min timepoint overlaid as a solid line. Error bars show 90% CI. Analysis of statistical significance at the 0.05 level was determined using one-way repeated measures ANOVA with Dunnett's correction post hoc. (A) RapR-Shp2 expressing cells had significant differences in protrusive activity means ($F[23,1] = 6.63$, $P < 0.001$). There was significant difference in means for time points 20–170 min relative to the 0 min time point. FRB expressing cells did not show significant changes in protrusive activity at the 0.05 level ($F[23,1] = 1.27$, $P = 0.184$). (B) RapR-Shp2 expressing cells had significant differences in retraction activity means ($F[23,1] = 9.40$, $P < 0.001$). There was significant difference in means for time points 40–130 and 150–180 min relative to the 0 min time point. FRB expressing cells retraction activity was not significant at the 0.05 level ($F[23,1] = 1.10$, $P = 0.337$). (C and D) Analysis of morphological changes induced by CA-Shp2. HeLa cells transiently expressing CA-Shp2-mVenus were stained with CellMask Deep Red membrane marker, imaged live and analyzed as in Fig. 4. $N = 30$ cells, three independent biological replicates. Significance was determined via two-tailed Student's t test with $\alpha = 0.05$, n.s. is nonsignificant. (C) Cell area analysis binned over 1 h intervals. (D) Changes in cell migration determined by path length over 1 h intervals. Box and whisker plots: Box indicates first through third quartile with median line, whiskers are 10–90%, open square represents mean. (E) Representative images of RapR-Shp2-mVenus and mCherry-ipep-FRB after rapamycin addition or CA-Shp2-mVenus localization in HeLa cells.

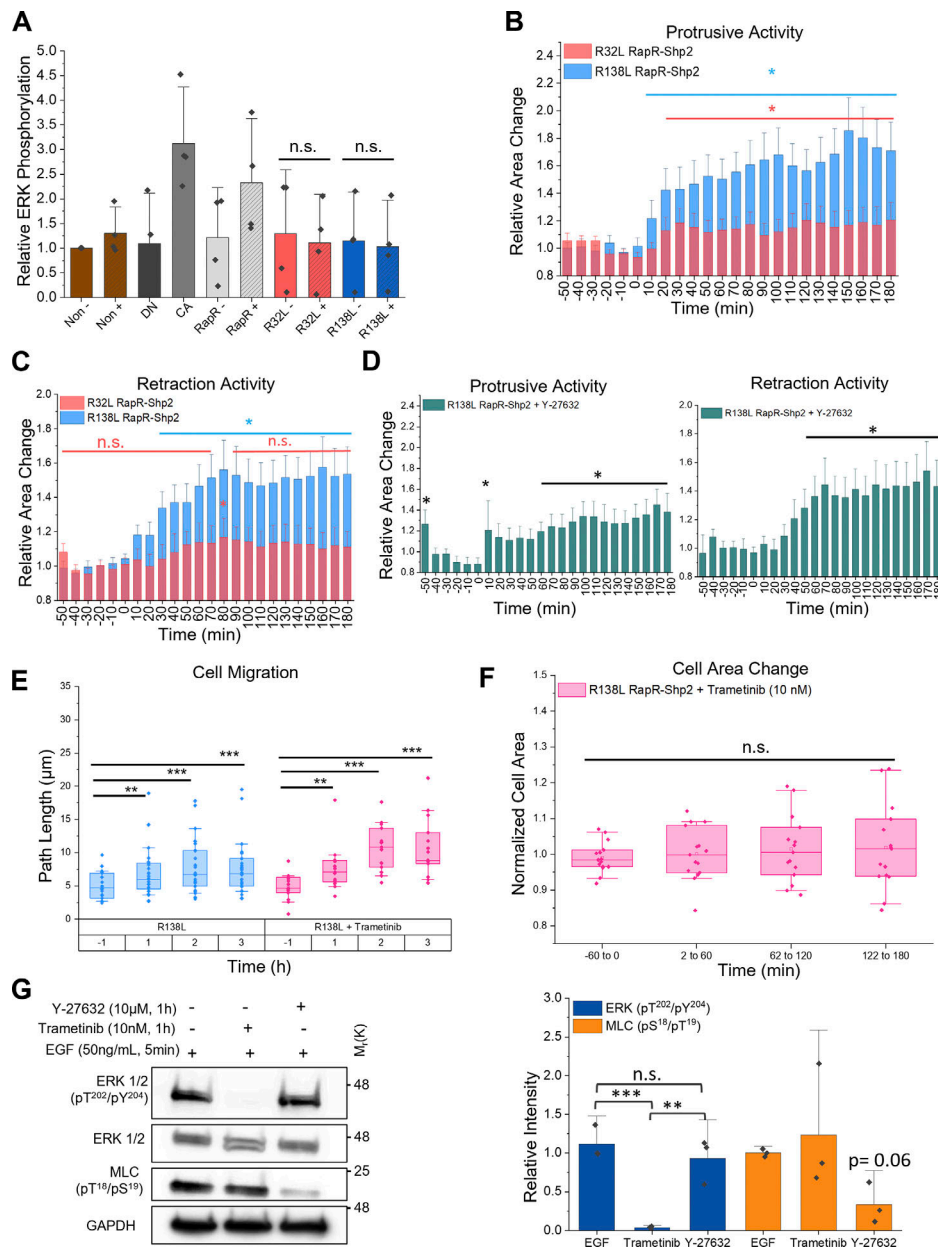


Figure S3. Role of SH2 domains of Shp2 in mediating ERK activation and ROCK II-dependent cell migration. (A) Analysis of Western blot intensity for ERK activation following RapR-Shp2 stimulation (Fig. 7 A). All phospho-ERK (pT²⁰²/pY²⁰⁴) signals are normalized to total ERK blot intensity and to the signal for nontransfected cells not treated with rapamycin. Statistical significance was determined using two-tailed Student's *t* test comparing independent SH2 domain mutants with and without rapamycin. (B–E) HeLa cells transiently expressing R32L or R138L RapR-Shp2 and mCherry-FRB were stained with CellMask Deep Red membrane marker and imaged live, data from Fig. 7. CellMask images were used for analysis of morphological changes. (B–D) Protrusive (B) and Retraction (C) activity of HeLa cells expressing R32L RapR-Shp2 (rose), R138L RapR-Shp2 (cyan), or (D) R138L RapR-Shp2 pretreated with 10 μM Y-27632 (teal). Bar graph shows activity binned over 10 min intervals. (B and D) There were significant differences in protrusive activity means for R32L RapR-Shp2 expressing cells (rose, $F[23,1] = 3.74$, $P < 0.001$), R138L RapR-Shp2 expressing cells (cyan, $F[23,1] = 17.67$, $P < 0.001$), and R138L RapR-Shp2 pretreated with Y-27632 (teal, $F[23,1] = 6.75$, $P < 0.001$). (C and D) There were significant differences in retraction activity means for R32L RapR-Shp2 expressing cells (rose, $F[23,1] = 3.04$, $P < 0.001$), R138L RapR-Shp2 expressing cells (cyan, $F[23,1] = 21.81$, $P < 0.001$), and R138L RapR-Shp2 pretreated with Y-27632 (teal, $F[23,1] = 12.24$, $P < 0.001$). (E) Changes in cell migration induced by activation of R138L RapR-Shp2 in the absence (cyan, data from Fig. 7 D) and presence (pink, $F[3,1] = 19.92$, $P < 0.001$) of 10 nM trametinib. Box plot indicates path length over 1 h. (F) Cell area change in response to R138L RapR-Shp2 activation following treatment with trametinib ($F[3,1] = 1.27$, $P = 0.295$), binned over 1 h intervals. (G) Representative immunoblot of HeLa cells pretreated with 10 nM Trametinib or 10 μM Y-27632 for 1 h and activated with EGF for 5 min. Immunoblot of ERK 1/2 (pT²⁰²/pY²⁰⁴), total ERK 1/2, Myosin Light Chain 2 (pT¹⁸/pS¹⁹), and total Myosin Light Chain 2. (right) Quantification of signal intensities for phospho-ERK normalized to total ERK ($F = 22.66$, $P = 0.002$) and phospho-Myosin Light Chain 2 normalized to GAPDH ($F = 2.77$, $P = 0.14$). $N = 3$ independent biological replicates. Analysis of statistical significance at the 0.05 level was determined using one-way ANOVA with Holm-Bonferroni correction for pairwise comparisons. Error bars in A–D and G show 90% CI. (B–F) Analysis of statistical significance at the 0.05 level was determined using one-way repeated measures ANOVA with Dunnett's correction post hoc relative to basal (–1 h, –60 to 0 min, 0 min). * $P < 0.05$, ** $P < 0.01$, *** $P < 0.001$. Box and whisker plots in E and F: Box indicates first through third quartile with median line, whiskers are 10–90%, and open square represents mean.

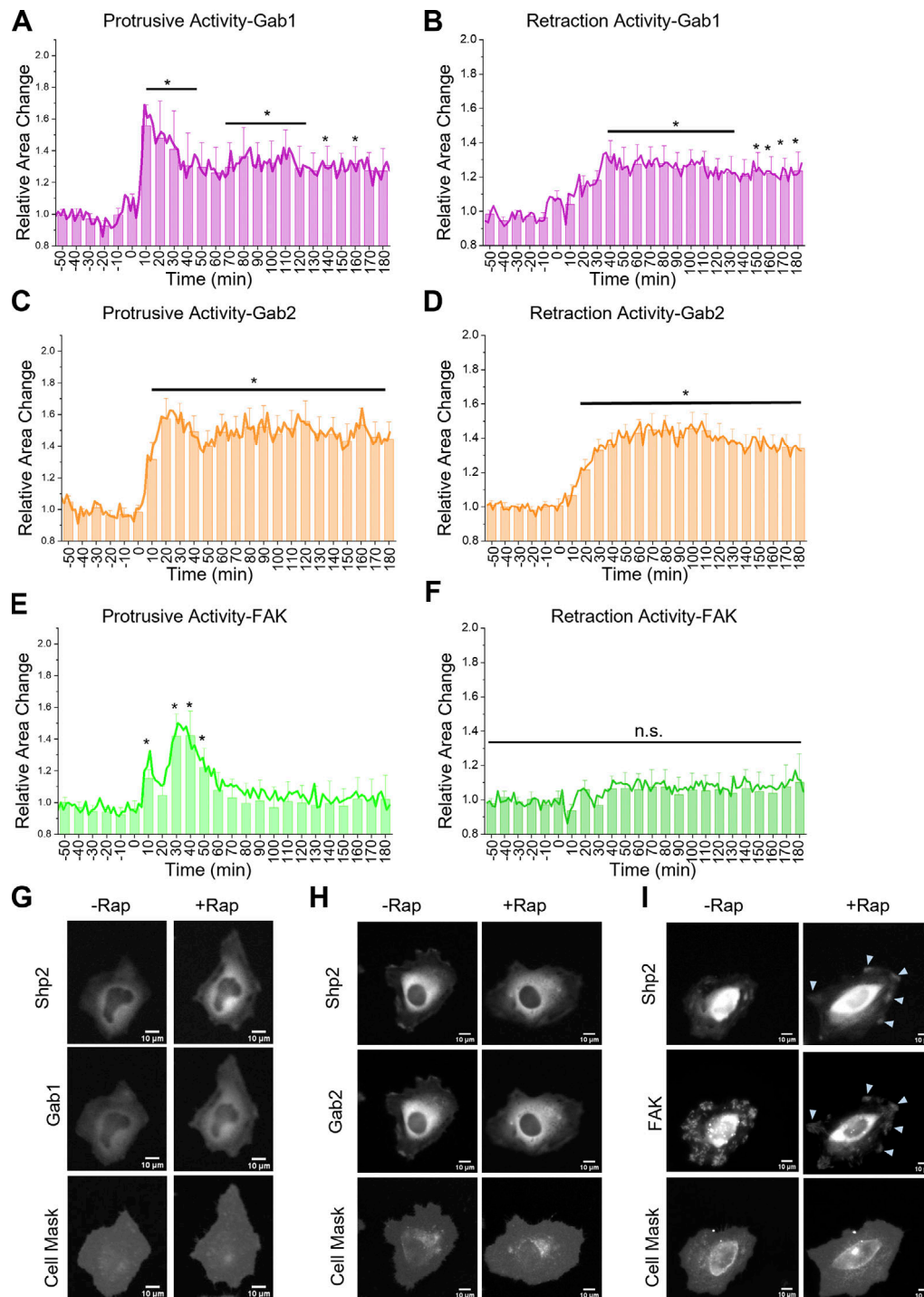


Figure S4. **Protrusion and Retraction analysis for RapRTAP-Shp2.** HeLa cells transiently expressing R32L RapR-Shp2-cerulean-flag and the FRB fused target protein were stained with CellMask Deep Red membrane dye and imaged live, data from Fig. 8. CellMask images were used to determine protrusive and retraction activity binned over 10 min intervals with mean activity at each 2 min time point overlaid as a solid line, error bars show 90% CI. Addition of Rapamycin at time 0 min. Analysis of statistical significance at the 0.05 level was determined using one-way repeated measures ANOVA with Dunnett's correction relative to the 0 min time point post hoc. **(A and B)** Analysis of changes in Protrusive (A) and Retraction (B) activity induced by targeted activation of RapR-Shp2 in complex with Gab1 showed significant changes in protrusion ($F[23,1] = 9.0, P < 0.001$) from time points 10–50 min, 70–120, 140 and 160 min and significant changes in retraction ($F[23,1] = 14.04, P < 0.001$) from time points 40–130 and 150–180 min. **(C and D)** Analysis of changes in Protrusive (C) and Retraction (D) activity induced by targeted activation of RapR-Shp2 in complex with Gab2 showed significant changes in protrusion ($F[23,1] = 28.29, P < 0.001$) from time points 10–180 min and significant changes in retraction ($F[23,1] = 40.46, P < 0.001$) from time points 20–180 min. **(E and F)** Analysis of changes in Protrusive (E) and Retraction (F) activity induced by targeted activation of RapR-Shp2 in complex with FAK showed significant changes in protrusion ($F[23,1] = 8.95, P < 0.001$) from time points 10 and 30–50 min and no significant changes in retraction ($F[23,1] = 1.33, P = 0.139$). **(G–I)** Representative images HeLa cells stained with CellMask Deep Red and transfected with R32L RapR-Shp2-cerulean (Shp2) and indicated FRB fusion proteins before and after rapamycin treatment. Focal adhesions with localized Shp2 are indicated with blue arrows.

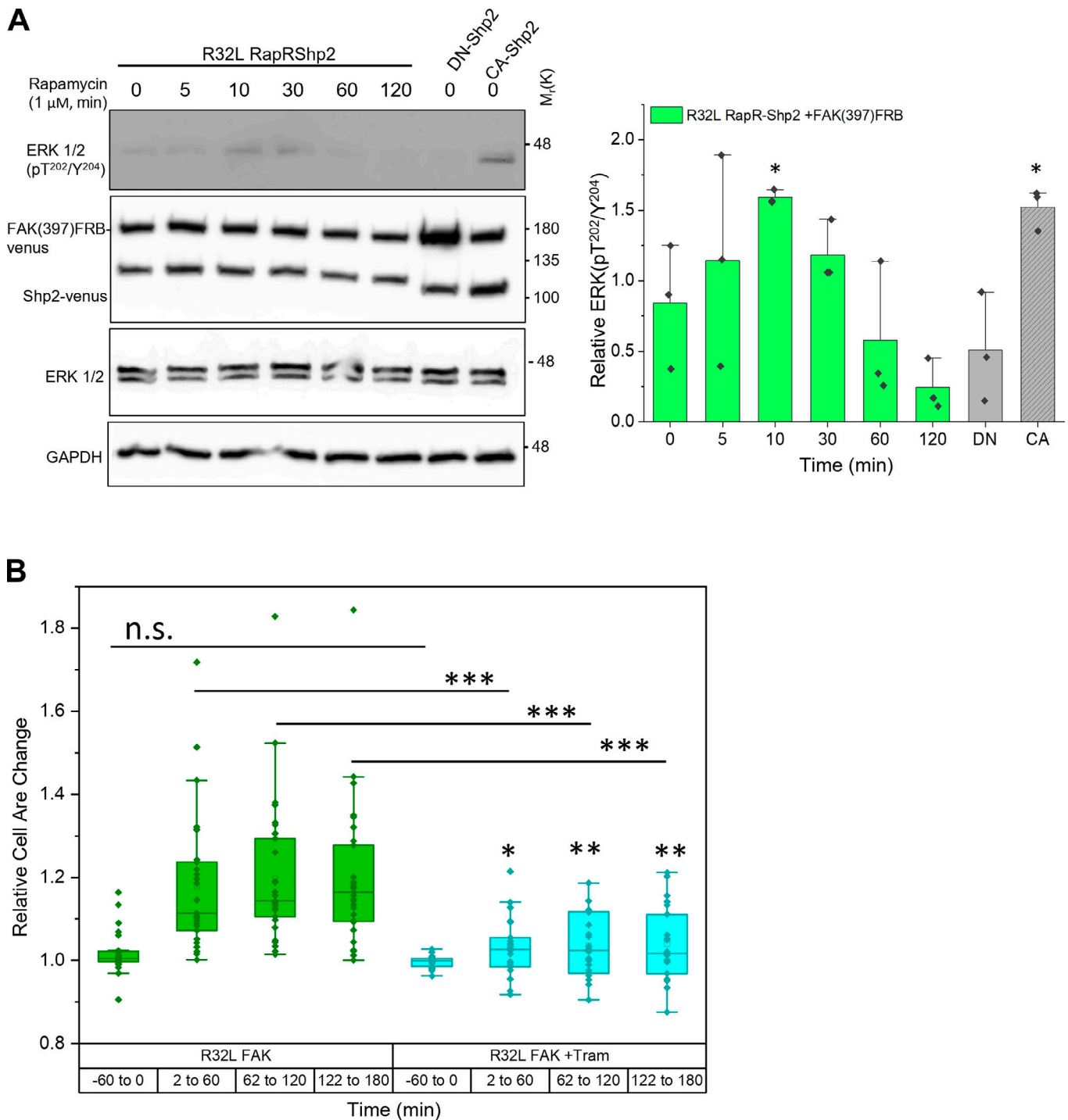


Figure S5. **Shp2 activation in focal adhesions results in transient ERK activation and ERK-dependent spreading.** (A) HEK293T cells transiently expressing FAK(397)FRB-mVenus coexpressed with R32L RapR-Shp2-mVenus, CA-Shp2-mVenus, or DN-Shp2-mVenus were treated with rapamycin for indicated time and analyzed for phosphorylation of ERK1/2. Representative blots of $N = 3$ biological replicates. Right: Quantification of phospho-ERK signal normalized to total ERK signal and to the 0 min time point. Error bars show 90% CI. Analysis of statistical significance at the 0.05 level was determined using one-way repeated measures ANOVA with Dunnett's correction post hoc relative to basal (0 min). Significant difference in the means was observed ($F[7,1] = 9.33$, $P < 0.01$). * $P < 0.05$. (B) HeLa cells transiently expressing R32L RapR-Shp2 and FAK(397)-FRB were stained with CellMask Deep Red membrane marker and imaged for 4 h every 2 min. Cells were pretreated with Trametinib (10 nM) for 1 h prior to imaging. Rapamycin was added at 0 min. Normalized change in cell area was binned over 1 h intervals. The area of R32L RapR-Shp2 targeted to FAK(397)-FRB in the absence of trametinib (green, data from Fig. 8 C) plotted against R32L RapR-Shp2 targeted to FAK(397)-FRB with trametinib treatment (cyan, $F[3,1] = 4.69$, $P = 0.005$; $N = 22$ cells, three independent biological replicates). Treatment with trametinib significantly influenced cell spreading vs FAK targeting without treatment ($F[3,1] = 15.69$, $P < 0.001$). Box and whisker plots: Box indicates first through third quartile with median line, whiskers are 10–90%, and open square represents mean. To evaluate the effect of RapR-Shp2 versus each inhibitor two-way repeated measures ANOVA with Holm-Bonferroni correction was performed for pairwise analysis of each time point for R32L RapR-Shp2 targeted to FAK with and without Trametinib. * $P < 0.05$, ** $P < 0.01$, *** $P < 0.001$.

Video 1. **RapR-Shp2 induced cell protrusions and migration.** HeLa cell coexpressing RapR-Shp2-mVenus-flag and mCherry-ipep-FRB and stained with CellMask Deep Red membrane marker. CellMask Deep Red was imaged for 4 h every 2 min. Rapamycin (1 μ M) was added at 60 min (indicated by appearance of "Rapamycin" sign).

Video 2. **RapR-Shp2 activation and targeting to Gab1.** HeLa cell coexpressing R32L RapR-Shp2-Cerulean-flag and FRB-GFP-Gab1 (Y628F/Y660F) were stained with CellMask Deep Red membrane marker dye and imaged live. CellMask Deep Red was imaged for 4.5 h every 2 min. Rapamycin (1 μ M) was added at 90 min (indicated by appearance of "Rapamycin" sign).

Video 3. **RapR-Shp2 activation and targeting to Gab2.** HeLa cell coexpressing R32L RapR-Shp2-Cerulean-flag and FRB-GFP-Gab2 (Y604F/Y634F) were stained with CellMask Deep Red membrane marker and imaged live. CellMask Deep Red was imaged for 4.5 h every 2 min. Rapamycin (1 μ M) was added at 90 min (indicated by appearance of "Rapamycin" sign).

Video 4. **RapR-Shp2 activation and targeting to FAK.** HeLa cell coexpressing R32L RapR-Shp2-Cerulean-flag and FAK(397)FRB-mVenus were stained with CellMask Deep Red membrane marker and imaged live. CellMask Deep Red was imaged for 4.5 h every 2 min. Rapamycin (1 μ M) was added after 90 min (indicated by appearance of "Rapamycin").

Video 5. **(R138L) RapR-Shp2 in focal adhesions combines two parallel signaling pathways.** HeLa cell coexpressing R138L RapR-Shp2-Cerulean-flag and FAK(397)FRB-mVenus with CellMask Deep Red membrane marker. CellMask Deep Red mask imaged for 4.5 h every 2 min. Rapamycin (1 μ M) was added after 90 min (indicated by appearance of "Rapamycin").